Comput Mech (2013) 52:377–399
DOI 10.1007/s00466-012-0818-3

ORIGINAL PAPER

Three-dimensional finite rotations treatment based on a minimal set parameterization and vector space operations in beam elements

Salvatore Lopez

Received: 29 February 2012 / Accepted: 17 November 2012 / Published online: 9 December 2012

Abstract A minimal set vectorial parameterization involving vector space operations is proposed for finite 3D rotations in structural analysis. In this approach, based on the updated Lagrangian description, complex manipulations required to obtain conservative descriptions and well-posed transformation matrices are avoided. In particular, slopes are used instead of rotation parameters to compute the nonlinear representations of the strain measures in the inertial frame of reference. This approach is applied to a geometrically nonlinear formulation for 3D beam elements in the hypotheses of large rotations and small strains. Numerical tests have been carried out to validate the developed technique in the frame structures context.

Keywords Nonlinear three-dimensional beam analysis · Finite elements · Finite rotations · Vectorial parameterization

1 Introduction

Considerable work has been devoted to developing models for 3D elastic frame structures for small strains and in the presence of large rotations. In this context, the co-rotational is one of the classical approaches used. The motion of the continuous medium is decomposed into a rigid body motion followed by a pure deformation. For this reason, the finite element is studied in the linear case where clearly drawbacks appear. Then, the nonlinear motion is obtained by joining the linear kinematic with a rigid body motion that is recovered by the use of orthogonal transformation matrices. The evolution of the co-rotational approach can be traced by referring to the works of Stuelpnagel [37], Belytschko and Hsieh [5], Goldstein [15], Argyris [1], Rankin and Nour-Omid [32], Cardona and Geradin [9], Crisfield [11], Atluri and Cazzani [3], Geradin and Rixen [14], Ibrahimbegović et al. [19] and Felippa [13].

The large-scale calculations required by these formulations have encouraged efficient treatments of the finite rotations. Those treatments, typically based on the rotation vector of the Euler theorem to describe finite rotations, have an economical definition of the rotated local reference system because only three parameters are used. Such a minimal set approach for the parameterization of the rotations, however, suffers from the singularities in the transformation matrices for several angles and requires complex manipulations to overcome nonconservative descriptions. In effect, in the use of updated Lagrangian procedures, the composition of rotations is required while rotation vectors cannot be added together. As a result an inverse problem must be solved to recover admissible variations of the rotation vector or case statements must be used in the coding. Formulations based on finite rotation updates in incremental-iterative procedures can be found in Ibrahimbegović and Al Mikdad [18] and Yang et al. [40]. Recently, an algorithm where the solution of the inverse problem is not case sensitive was set out in Pimenta et al. [31] and Campello et al. [8].

As stated, the singularities for arbitrarily large rotations are not just inherent in the co-rotational approach, but in all methods based on a minimal set of parameters. The choice of the three parameters, therefore, is usually made by considering the characteristics of a specific application, without however avoiding singularities. In the quaternion descriptions, free singularity parameterizations can be obtained by adding a further parameter, and subjecting the related Lagrange multiplier to a constraint equation. Besides, more nonlinear equations have to be solved while computationally expensive

S. Lopez (✉)
Dipartimento di Modellistica per l'Ingegneria, Università della Calabria, 87030 Rende, Italy
e-mail: salvatore.lopez@unical.it

evaluations of the coefficients in the force vector and in the tangent stiffness matrix persist.

Total Lagrangian approaches have also been developed. In a first alternative, slopes are used instead of rotation parameters. In the absolute nodal coordinate formulation (see Sopanen and Mikkola [35], Dufva et al. [12], Sugiyama et al. [38]) the cross-section orientation of the element in the frame of reference is defined by position vector gradients. A similar vectorial finite element approach (Rhim and Lee [33]) defines the cross-section in the 3D space by two vectors that take warping into account. However, due to the use of a cross-sectional coordinate system, the rigid cross-section assumption is abandoned while the description of the elastic forces becomes more complex. A second alternative is represented by the use of low-order 3D finite elements based on definitions of relative lengths only (see [25,28]). In this approach, strains are computed by making them linear independent and invariant to the rigid kinematics measures.

More recently, formulations where the nonlinear rigid motion is recovered by referring to three unit and mutually orthogonal vectors attached to the elements have been presented. All nine components of such vectors in the global inertial frame of reference are assumed as unknown and the rotational degree of freedom of the element is reduced to only three by six constraint conditions. In the works of Betsch and Steinmann [6,7] orthonormality of the directors is enforced by using six scalar products. In particular, three unit length and three orthogonality conditions are imposed on the directors by using the scalar products among them and reciprocally, respectively. In [26] and [27], instead, three scalar products and one cross product are used to define the constraint conditions. In particular, one orthogonality and two unit length conditions are imposed by scalar products while the complete definition of a director is obtained by referring to a cross product. Hence, the formulation proves to be well posed for any finite rotations.

In this paper we present a minimal set approach for the parameterization of the rotations in the context of updated Lagrangian descriptions. Such an approach is based on that used in [26] and [27] for the statical and dynamical geometrically nonlinear analysis of beams. Here, the use of the internal constraint equations is replaced by the intrinsic definition of the related rotation parameters by obtaining a three parameter description. We demonstrate that such a reduction from nine to three unknown components is well posed under widely applicable hypotheses. The resulting formulation still involves vector space operations for the description of the finite 3D rotations while algorithmical formulation is simple and evaluations of the coefficients in the force vector and in the tangent stiffness matrix are inexpensive.

As regards beam element modeling, here we use a small strain - finite displacement formulation of a two-node finite element based on the Timoshenko beam theory. The actual configuration of the element is rigidly translated and rotated, and deformed according to selected linear modes. Rigid and deformation modes are referred to the nodes at the boundaries of the element with six unknowns per node. The nonlinear motion is recovered by referring to three unit and mutually orthogonal vectors attached to the nodes. As stated, three of the nine components of such vectors in the global inertial frame of reference are assumed as unknown. Afterward, the deformative modes are summed up in the strain tensor definition.

We note that boundary conditions on rotations are imposed by assuming as known the related nodal slopes while applied moments are modelled as forces following the motions. It follows that, as will be discussed later, treatment of rotational boundary conditions and external moments proves to be slightly more complex with respect to the co-rotational formulations. Furthermore, the incremental rotations are restricted to the range of validity of the described parametrization. Overall, however, the use of the presented formulation requires less implementation effort and arithmetical operations with respect to the classical one.

The paper is set out in the following way. In Sects. 2 and 3 we describe the update treatment of rotations by slopes and angles respectively. In Sect. 4 we define the kinematics of the beam element and the related energetic quantities are evaluated. Section 5 discusses some aspects related to the variational formulation and related linearization. Section 6, after defining the treatment of applied moments and boundary conditions, contains the description of the nonlinear problem and the related solution algorithm. Several numerical examples that compare the described formulations based on slopes and angles for the rotation parametrization are presented in Sect. 7 and final conclusions are drawn in Sect. 8. The regularity of the augmented constrained problem is demonstrated in Appendix 1.

2 Update treatment of rotations by slopes

In the following, we refer to Fig. 1 and we denote with Latin indices i and j the values $[1, \ldots, 3]$ while δ_{ij} is the Kronecker delta. Let $\mathbf{g}_i = \{g_{ij}\}$ and $\hat{\mathbf{g}}_i = \{\hat{g}_{ij}\}$ be, respectively, the actual and the initial configuration of three unit mutually orthogonal vectors in the inertial reference basis $\mathbf{k}_i = \{k_{ij}\} = \{\delta_{ij}\}$. Matrix $\hat{\mathbf{G}}$ links $\hat{\mathbf{g}}_i$ and $\mathbf{k}_i$ vectors by $\hat{\mathbf{g}}_i = \hat{\mathbf{G}}\mathbf{k}_i$ while $\mathbf{G}$ maps $\hat{\mathbf{g}}_i$ into $\mathbf{g}_i$ vectors by $\mathbf{g}_i = \mathbf{G}\hat{\mathbf{g}}_i$.

Now let $\bar{\mathbf{g}}_i = \{\bar{g}_{ij}\}$ be an intermediate configuration of the $\mathbf{g}_i$ vectors and $\bar{\mathbf{e}}_i = \{\bar{e}_{ij}\}$ the related representation in the $\hat{\mathbf{g}}_i$ basis. Analogously, $\mathbf{e}_i = \{e_{ij}\}$ is the counterpart of $\mathbf{g}_i$ in the $\bar{\mathbf{g}}_i$ reference. So the $\bar{\mathbf{E}} = [\bar{\mathbf{e}}_1|\bar{\mathbf{e}}_2|\bar{\mathbf{e}}_3]$ and $\mathbf{E} = [\mathbf{e}_1|\mathbf{e}_2|\mathbf{e}_3]$ matrices describe the tranformations $\bar{\mathbf{g}}_i = \bar{\mathbf{E}}\hat{\mathbf{g}}_i$ and $\mathbf{g}_i = \mathbf{E}\bar{\mathbf{g}}_i$, respectively. Note that $\{\bar{e}_{ij}\}$ or $\{e_{ij}\}$ reduce to $\{\delta_{ij}\}$ if basis $\bar{\mathbf{g}}_i$ coincides with $\hat{\mathbf{g}}_i$ or $\mathbf{g}_i$ with $\bar{\mathbf{g}}_i$.

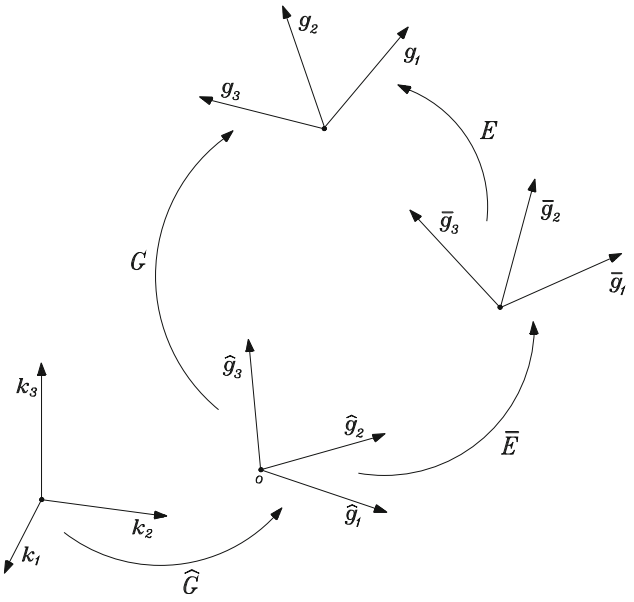

Fig. 1 Unit base vectors: configurations and related mappings

In the approach described in the work [26] the g_{ij} components of the $\mathbf{g}_i$ vectors are assumed as unknown parameters. The nine g_{ij} unknown components are subject to six constraint conditions so that the related direction cosine matrix $\mathbf{G} = [\mathbf{g}_1|\mathbf{g}_2|\mathbf{g}_3]$ is orthogonal, i.e. $\mathbf{G}\mathbf{G}^T = \mathbf{G}^T\mathbf{G} = \mathbf{I}$, with $\mathbf{I}$ as identity matrix. In Appendix 1 we give the proof that the rotational degrees of freedom are reduced to just three and the constraint conditions are well posed for unbounded rotations. We outlined that the imposition of the constraint conditions on the e_{ij} unknown components introduces the terms related to the Lagrange multipliers. The computation of these contributions to the internal force vector and to the tangent stiffness matrix is simple to perform while a nodal process is followed for the derivative of the related extended functional with respect to the Lagrange multipliers. However nine slopes plus six Lagrange multiplier unknowns are used for the description of each rotated cross-section.

Here we abandon the unbounded validity for finite rotations of the cited method so reducing the description to a minimal set of parameters. In effect, under widely applicable hypotheses on the $\mathbf{e}_i$ incremental vectors from the updated $\bar{\mathbf{e}}_i$ ones, by the cited conditions

$$\begin{aligned}
&\mathbf{e}_2 \cdot \mathbf{e}_3 = 0,\\
&\mathbf{e}_2 \cdot \mathbf{e}_2 - 1 = 0,\\
&\mathbf{e}_3 \cdot \mathbf{e}_3 - 1 = 0,\\
&\mathbf{e}_2 \times \mathbf{e}_3 = \mathbf{e}_1,
\end{aligned} \tag{1}$$

here we give an explicit definition of the e_{ij} components as a function of the e_{21}, e_{31} and e_{32} parameters. To demonstrate that such a reduction is well posed we proceed in a constructive manner.

Of course, by the fourth of the (1) conditions, the cross product between the $\mathbf{e}_2$ and $\mathbf{e}_3$ directors is an explicit definition of the components e_{11}, e_{12} and e_{13} of the $\mathbf{e}_1$ director for any rotation. We assume $1 - e_{31}^2 - e_{32}^2 > 0$ and $e_{33} > 0$ so that

$$e_{33} = \sqrt{1 - e_{31}^2 - e_{32}^2} \tag{2}$$

is obtained directly by the $\mathbf{e}_3$ unit length condition. By the first of (1), then, the expression

$$e_{23} = -\frac{e_{21}e_{31} + e_{22}e_{32}}{e_{33}} \tag{3}$$

is well posed. Inserting (3) into the second of (1) and defining

$$\Delta = e_{33}^2 + e_{32}^2 - e_{21}^2 \ (e_{31}^2 + e_{32}^2 + e_{33}^2) = e_{33}^2 + e_{32}^2 - e_{21}^2 \tag{4}$$

we have

$$\begin{aligned}
e_{22} &= \frac{-e_{21}e_{31}e_{32} + e_{33}\sqrt{\Delta}}{e_{32}^2 + e_{33}^2} \quad \text{or}\\
e_{22} &= \frac{-e_{21}e_{31}e_{32} - e_{33}\sqrt{\Delta}}{e_{32}^2 + e_{33}^2}
\end{aligned} \tag{5}$$

if the further condition $\Delta > 0$ is satisfied as $e_{32}^2 + e_{33}^2 \neq 0$ due to $e_{33} > 0$. Apart from the choice of the two solutions given in (5), the reduction in unknown parameters by the (1) conditions is realized. In effect, by inserting the e_{33} expression of (2) in (3) and (5) we obtain the expression of the components of the $\mathbf{e}_2$ and $\mathbf{e}_3$ vectors as a function of the e_{21}, e_{31} and e_{32} assumed parameters. Then, the components of the $\mathbf{e}_1$ vector are also defined.

Now let θ_{ij} and $\pi/2 + \theta_{ij}$ be the angles between $\mathbf{e}_i$ and $\bar{\mathbf{e}}_j$ vectors for $i = j$ and $i \neq j$, respectively. So $e_{ij} = \cos\theta_{ij}$ for $i = j$ while $e_{ij} = \sin\theta_{ij}$ for $i \neq j$. Suppose that $\theta_{ij} \in (-\theta^*, +\theta^*)$ with $\theta^* = \arcsin(\sqrt{2}/2) = 0.785398\text{rad} = 45^o$. Then we verify that

$$\begin{aligned}
&0 = 1 - 2\sin^2\theta^* < 1 - e_{31}^2 - e_{32}^2 < 1,\\
&\text{and} \quad 0 < \cos\theta^* < e_{33} < 1.
\end{aligned} \tag{6}$$

As $\mathbf{e}_3$ is a unit length vector, with (4) we can write $\Delta = 1 - e_{31}^2 - e_{21}^2$. Additionally, exploiting $\mathbf{E}\mathbf{E}^T = \mathbf{I}$, we obtain the expression $\Delta = e_{11}^2$. Then

$$\cos^2\theta^* < \Delta < 1. \tag{7}$$

We denote respectively with e_{22}^+ and e_{22}^- the first and the second solution given in (5). By referring to the θ_{ij} angles, then

$$e_{22}^{\pm} = \frac{-\sin\theta_{21}\sin\theta_{31}\sin\theta_{32} \pm \cos\theta_{33}\cos\theta_{11}}{1 - \sin^2\theta_{31}}. \tag{8}$$

By the (7) bounds, evaluations on the $e_{22}^{\pm}$ coefficients give

$$\begin{aligned}
&-\sin^3\theta^* + \cos^2\theta^* < e_{22}^+ < (\sin^3\theta^* + 1)/(1 - \sin^2\theta^*),\\
&-\sin^3\theta^* - 1 < e_{22}^- < (\sin^3\theta^* - \cos^2\theta^*)/(1 - \sin^2\theta^*).
\end{aligned} \tag{9}$$

As we can verify by the (9) inequalities we have $e_{22}^{+} > 0$ and $e_{22}^{-} < 0$. As e_{22} is in the range $(\cos(-\theta^*), \cos(\theta^*))$ the choice $e_{22} = e_{22}^{+}$ must be made.

Then, in the formulation θ^* proves to be the singularity value for the rotational parameters. However, as at present the formulation is based on the updated Lagrangian procedure, such a value is not a restricting bound.

To obtain the updated treatment of rotations we refer to the following expression for the actual configuration of the $\mathbf{g}_i$ orthonormal triad at the k-th step

$$\mathbf{g}_{i(k)} = \mathbf{G}_{(k)}\hat{\mathbf{g}}_i, \qquad \mathbf{G}_{(k)} = \mathbf{E}_{(k)}\bar{\mathbf{E}}_{(k)}. \tag{10}$$

Vectors $\mathbf{e}_{i(k)}$ defining $\mathbf{E}_{(k)}$ in (10), as stated, represent the incremental rotation from the $\bar{\mathbf{e}}_{i(k)}$ previously computed configuration. The subsequent $k+1$ step, afterward, refers to the

$$\bar{\mathbf{E}}_{(k+1)} = \mathbf{E}^*_{(k)}\bar{\mathbf{E}}_{(k)},\ \bar{\mathbf{E}}_{(k+1)} = \left[\begin{array}{c|c|c} \bar{\mathbf{e}}_{1(k+1)} & \bar{\mathbf{e}}_{2(k+1)} & \bar{\mathbf{e}}_{3(k+1)} \end{array}\right],$$
$$\mathbf{E}^*_{(k)} = \left[\begin{array}{c|c|c} \mathbf{e}^*_{1(k)} & \mathbf{e}^*_{2(k)} & \mathbf{e}^*_{3(k)} \end{array}\right] \tag{11}$$

updated configuration with the $\mathbf{e}^*_{i(k)}$ established configuration of $\mathbf{e}_i$. The process is initialized by $\bar{\mathbf{E}}_{(0)} = \mathbf{I}$.

As we can see, simple products are used recursively to compose as many successive rotations as necessary. In particular, the $\bar{\mathbf{E}}$ matrix takes into account the previously computed rotations of the $\hat{\mathbf{g}}_i$ in the $\bar{\mathbf{g}}_i$ frame while $\mathbf{e}_i$ vectors map $\bar{\mathbf{g}}_i$ in the actual $\mathbf{g}_i$ frame. In fact, we note that the updated values of rotational parameters are directly the $\bar{E}_{12}$, $\bar{E}_{13}$ and $\bar{E}_{23}$ coefficients of the (11) updated rotational matrix.

In the k-th step, vectors $\mathbf{e}_{i(k)}$ are completely defined as a function of the $e_{21(k)}$, $e_{31(k)}$ and $e_{32(k)}$ unknown parameters by the previously described expressions. In a continuation procedure, besides, the range $|\theta_{ij}| < \theta^*$ covers the possible incremental rotation so that the rotations in between two successively established configurations remain moderate. In particular, by simple algebraic manipulations of the previous expressions of the e_{ij} components, the recursive exact evaluations

$$\begin{aligned}
&h = 1/(1-e_{31}^2),\ c_1 = \sqrt{1-e_{21}^2-e_{31}^2},\\
&c_3 = \sqrt{1-e_{31}^2-e_{32}^2},\\
&e_{11} = c_1,\\
&e_{33} = c_3,\\
&e_{22} = -(e_{21}e_{31}e_{32} - c_1c_3)h,\\
&e_{23} = -(e_{21}e_{31}c_3 + c_1e_{32})h,\\
&e_{12} = -(e_{31}e_{32}c_1 + e_{21}c_3)h,\\
&e_{13} = -(e_{31}c_1c_3 - e_{21}e_{32})h,
\end{aligned}$$

are used. Also their second and fourth order approximations are tested in the numerical analyses.

We note that the asymptotic extrapolations of rotation matrix components are computationally less expensive than their exact expressions. Furthermore, to obtain an accurate description of the equilibrium points and an efficient behaviour of the continuation process, the updated configurations typically are not very distant.

3 Update treatment of rotations by angles

The treatment of rotations is now based on the recursive composition

$$\mathbf{g}_{i(k)} = \mathbf{R}_{(k)}\bar{\mathbf{R}}_{(k)}\hat{\mathbf{g}}_i, \tag{12}$$

where $\mathbf{R}_{(k)} = \mathbf{R}(\boldsymbol{\psi}_{(k)})$ with ψ_i components of $\boldsymbol{\psi}$ being the unknown rotation parameters. Following the description given before, $\mathbf{R}_{(k)}$ is the incremental rotation matrix which maps the updated frame $\bar{\mathbf{g}}_{i(k)}$ into the actual frame $\mathbf{g}_{i(k)}$ while $\bar{\mathbf{R}}_{(k)} = \bar{\mathbf{R}}_{(k)}(\bar{\boldsymbol{\psi}}_{(k)})$ maps the initial frame $\hat{\mathbf{g}}_i$ into the updated frame $\bar{\mathbf{e}}_{i(k)}$.

Based on the rotation vector $\boldsymbol{\psi} = \varphi\boldsymbol{\phi}$, $\boldsymbol{\phi}^T\boldsymbol{\phi} = 1$, of the Euler theorem to describe finite rotations, a representation of rotation operators is:

$$\mathbf{T}(\boldsymbol{\psi}) = \mathbf{I} + \frac{\sin\varphi}{\varphi}\boldsymbol{\Psi} + \frac{1-\cos\varphi}{\varphi^2}\boldsymbol{\Psi}^2, \tag{13}$$

where, if the trigonometric functions are expanded in Taylor series, we obtain the exponential map

$$\exp(\boldsymbol{\Psi}) = \mathbf{I} + \boldsymbol{\Psi} + \frac{1}{2}\boldsymbol{\Psi}^2 + \cdots. \tag{14}$$

In (13) and (14), $\boldsymbol{\Psi}$ denotes the skew symmetric tensor obtained by the components of vector $\boldsymbol{\psi}$:

$$\boldsymbol{\Psi} = \mathbf{Skew}(\boldsymbol{\psi}) = \begin{bmatrix} 0 & -\psi_3 & \psi_2 \\ \psi_3 & 0 & -\psi_1 \\ -\psi_2 & \psi_1 & 0 \end{bmatrix}. \tag{15}$$

The $\boldsymbol{\psi} = \mathbf{axial}(\boldsymbol{\Psi})$ is the converse operation of (15) that extracts the $\boldsymbol{\psi}$ vector from the skew symmetric tensor $\boldsymbol{\Psi}$.

In the use of the $\mathbf{G} = \mathbf{R}\bar{\mathbf{R}}$ composition of rotation operators, however, we stress that $\boldsymbol{\psi}_G \neq \boldsymbol{\psi} + \bar{\boldsymbol{\psi}}$ successive rotations cannot be obtained by simply adding their corresponding rotation vectors. Then, for a given $(\bar{\boldsymbol{\psi}}, \bar{\mathbf{R}})$ rotation, admissible $(\boldsymbol{\psi}_G, \mathbf{G})$ rotations are obtained if

$$\boldsymbol{\psi}_G = R^{-1}(\mathbf{G}). \tag{16}$$

The inverse problem (16) is defined as the operation of obtaining the $\boldsymbol{\psi}_G$ rotation vector based on the knowledge of the $\mathbf{G}$ rotation matrix. Such an operation can be obtained by the no ill-conditioning Spurrier algorithm [36]. The procedure, as presented in Simo and Vu-Quoc [34], is summarized here:

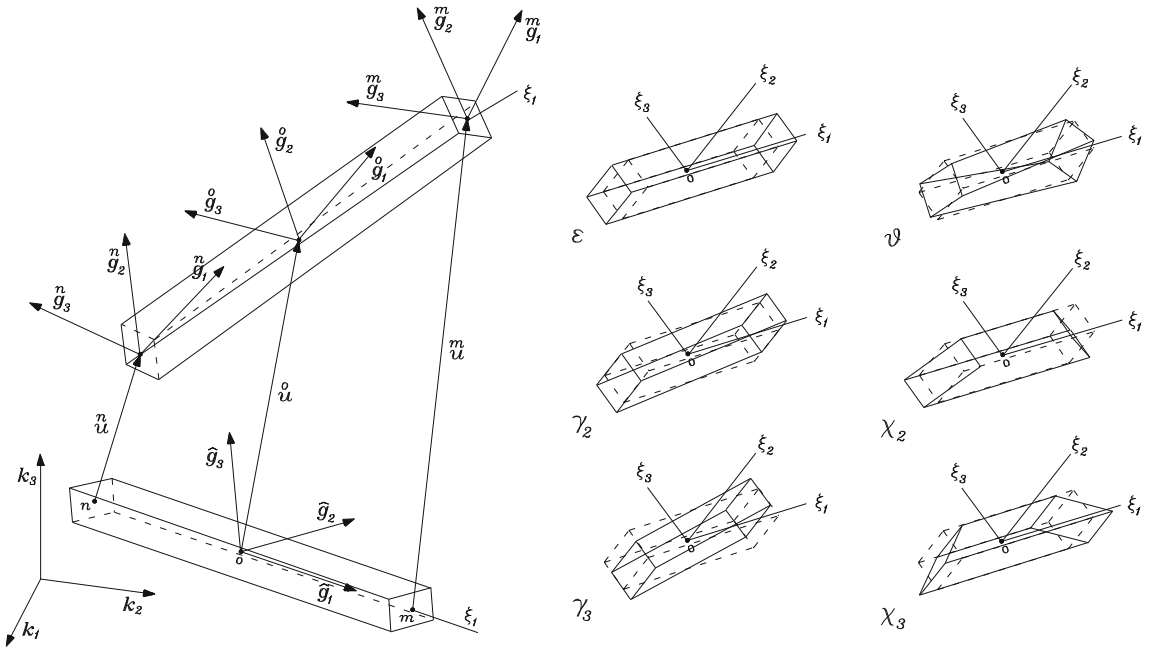

Fig. 2 Total Lagrangian co-rotational formulation: element kinematics and coordinate systems

1. $a = \max(G_{11}, G_{22}, G_{33}, G_{11} + G_{22} + G_{33})$;
2. case $a = G_{11} + G_{22} + G_{33}$:
   i. $\bar{q} = (1 + G_{11} + G_{22} + G_{33})^{1/2}/2$;
   ii. $q_i = -\sum_{jk} e_{ijk} G_{jk}/4\bar{q}, \quad i = 1, \ldots, 3$;
3. case $a \neq G_{11} + G_{22} + G_{33}, \quad a = G_{ii}$:
   i. $q_i = [G_{ii}/2 + (1 - G_{11} - G_{22} - G_{33})/4]^{1/2}$;
   ii. $\bar{q} = (G_{kj} - G_{jk})/4q_i, \quad q_j = (G_{ji} + G_{ij})/4q_i, \quad q_k = (G_{ki} + G_{ik})/4q_i$;
4. calculate $(\varphi_G, \boldsymbol{\psi}_G)$ through:
   i. $\varphi_G = 2 \arccos \bar{q}$;
   ii. $\psi_{Gi} = q_i \varphi_G / \sin(\varphi_G/2)$;

where i, j and k are the cyclic permutation of 1, 2 and 3, respectively, and e_{ijk} is the related permutation symbol. Computation 4.ii., finally, requires a further case depending to avoid numerical instabilities. Here the second order expansion $\varphi_G/\sin(\varphi_G/2) = 2 + \varphi_G^2/12$ is used when $|\varphi_G| < 0.001$.

In a highly simplified and computationally inexpensive approach to the successive composition of rotations, we can assume that the incremental $\mathbf{R}_{(k)}(\boldsymbol{\psi})$ operator in the composition (12) produces admissible rotations in the step. Explicitly, the following expressions for the coefficients of the $\mathbf{R}(\boldsymbol{\psi})$ incremental matrix are given by:

$$
\begin{aligned}
&\varphi = \sqrt{\psi_1^2 + \psi_2^2 + \psi_3^2}, \\
&s = \sin\varphi/\varphi, \; c = (1 - \cos\varphi)/\varphi^2, \\
&R_{11} = 1 - c\,(\psi_3^2 + \psi_2^2), \\
&R_{12} = -s\,\psi_3 + c\,\psi_2\psi_1, \\
&R_{13} = s\,\psi_2 + c\,\psi_3\psi_1, \\
&R_{21} = s\,\psi_3 + c\,\psi_2\psi_1, \\
&R_{22} = 1 - c\,(\psi_3^2 + \psi_1^2), \\
&R_{23} = -s\,\psi_1 + c\,\psi_3\psi_2, \\
&R_{31} = -s\,\psi_2 + c\,\psi_3\psi_1, \\
&R_{32} = s\,\psi_1 + c\,\psi_3\psi_2, \\
&R_{33} = 1 - c\,(\psi_2^2 + \psi_1^2).
\end{aligned}
$$

Second and fourth order approximations of the exponential map are also used in the tests. By referring to the established configuration $\boldsymbol{\psi}^*_{(k)}$, afterwards, the updated configuration is realized in the subsequent $k + 1$ step as

$$\mathbf{G} = \mathbf{R}^*_{(k)} \bar{\mathbf{R}}_{(k)}, \quad \boldsymbol{\psi}_G = R^{-1}(\mathbf{G}), \quad \bar{\mathbf{R}}_{(k+1)} = \mathbf{T}(\boldsymbol{\psi}_G). \tag{17}$$

The process is initialized by $\bar{\mathbf{R}}_{(0)} = \mathbf{I}$.

As stated, an algorithm where the solution of the inverse problem is not case sensitive can be found in [31] and [8]. The representation of the rotation operator is then given by

$$\mathbf{T}(\boldsymbol{\psi}) = \mathbf{I} + \frac{4}{4 + \varphi^2}\left(\boldsymbol{\Psi} + \frac{1}{2}\boldsymbol{\Psi}^2\right), \tag{18}$$

in contrast to (13) while the updated configuration is computed in the $k + 1$ step by using

$$\mathbf{G} = \mathbf{R}^*_{(k)}\bar{\mathbf{R}}_{(k)}, \quad \boldsymbol{\psi}_G = \frac{4}{4 - \boldsymbol{\psi}^{*T}\bar{\boldsymbol{\psi}}}(\boldsymbol{\psi}^* + \bar{\boldsymbol{\psi}} + \frac{1}{2}\boldsymbol{\psi}^* \times \bar{\boldsymbol{\psi}}),$$
$$\bar{\mathbf{R}}_{(k+1)} = \mathbf{T}(\boldsymbol{\psi}_G) \tag{19}$$

and $\bar{\mathbf{R}}_{(0)} = \mathbf{I}$. The coefficients of the $\mathbf{R}(\boldsymbol{\psi})$ incremental matrix are now obtained by using the (18) representation:

$$\begin{aligned}
&\varphi = \sqrt{\psi_1^2 + \psi_2^2 + \psi_3^2},\\
&h = 2/(4 + \varphi^2),\\
&R_{11} = 1 - (\psi_3^2 + \psi_2^2)h,\\
&R_{12} = (\psi_2\psi_1 - 2\psi_3)h,\\
&R_{13} = (\psi_3\psi_1 + 2\psi_2)h,\\
&R_{21} = (\psi_2\psi_1 + 2\psi_3)h,\\
&R_{22} = 1 - (\psi_3^2 + \psi_1^2)h,\\
&R_{23} = (\psi_3\psi_2 - 2\psi_1)h,\\
&R_{31} = (\psi_3\psi_1 - 2\psi_2)h,\\
&R_{32} = (\psi_3\psi_2 + 2\psi_1)h,\\
&R_{33} = 1 - (\psi_2^2 + \psi_1^2)h.
\end{aligned}$$

As before, also second and fourth order approximations of the (18) map are used in the numerical tests.

Note that expressions of the incremental rotation given in the previous section are computationally slightly less expensive than those given in this section because the three components e_{21}, e_{31} and e_{32} are assumed directly as unknowns. Such an advantage increases if more terms are added in the related expansions. In the slopes based formulation, furthermore, poor expansions can only compromise the approximation of the solution points while in the angles based formulations the admissibility of the incremental rotations is also compromised. An inverse problem to be solved or case statements, finally, are not present in the coding of the slopes based formulation.

4 Kinematics and energetic quantities of the beam element

Let ξ_1 be the referential coordinate along the beam element centerline $-h_1/2 \le \xi_1 \le +h_1/2$. In the following, we denote with n and m respectively the nodes in $\xi_1 = -h_1/2$ and $\xi_1 = +h_1/2$. Along the beam centerline we define the displacement vector $\mathbf{u}(\xi_1) = \{u_i(\xi_1)\}$ and the three orthonormal vectors $\mathbf{g}_1(\xi_1) = \{g_{1i}(\xi_1)\}$, $\mathbf{g}_2(\xi_1) = \{g_{2i}(\xi_1)\}$ and $\mathbf{g}_3(\xi_1) = \{g_{3i}(\xi_1)\}$ in the global inertial frame of reference $\mathbf{k}_i$. Director vectors $\mathbf{g}_2$ and $\mathbf{g}_3$ are along the principal axes of inertia of the cross-section ξ_2 and ξ_3, respectively. The initial unit vector in the ξ_i element direction, as before, will be denoted by $\hat{\mathbf{g}}_i$ (see Fig. 2).

In the beam element, global displacement vector $\mathbf{u}(\xi_1)$ is composed of rigid and deformation components. In particular, we refer to the $\bar{\mathbf{u}} = \{\bar{u}_i(\xi_1)\}$ rigid displacements defined in the initial frame of reference while the deformation $\tilde{\mathbf{u}}(\xi_1) = \{\tilde{u}_i(\xi_1)\}$ displacements and $\tilde{\boldsymbol{\varphi}}(\xi_1) = \{\tilde{\varphi}_i(\xi_1)\}$ rotations are defined in the local rigidly rotated frame of reference. The deformation kinematics is assumed by the linear interpolations

$$\tilde{u}_1 = \varepsilon\xi_1, \qquad \tilde{u}_2 = \gamma_2\xi_1, \qquad \tilde{u}_3 = \gamma_3\xi_1 \tag{20}$$

for displacements and

$$\tilde{\varphi}_1 = \theta\xi_1, \qquad \tilde{\varphi}_2 = \chi_3\xi_1, \qquad \tilde{\varphi}_3 = \chi_2\xi_1 \tag{21}$$

for torque and flexural rotations.

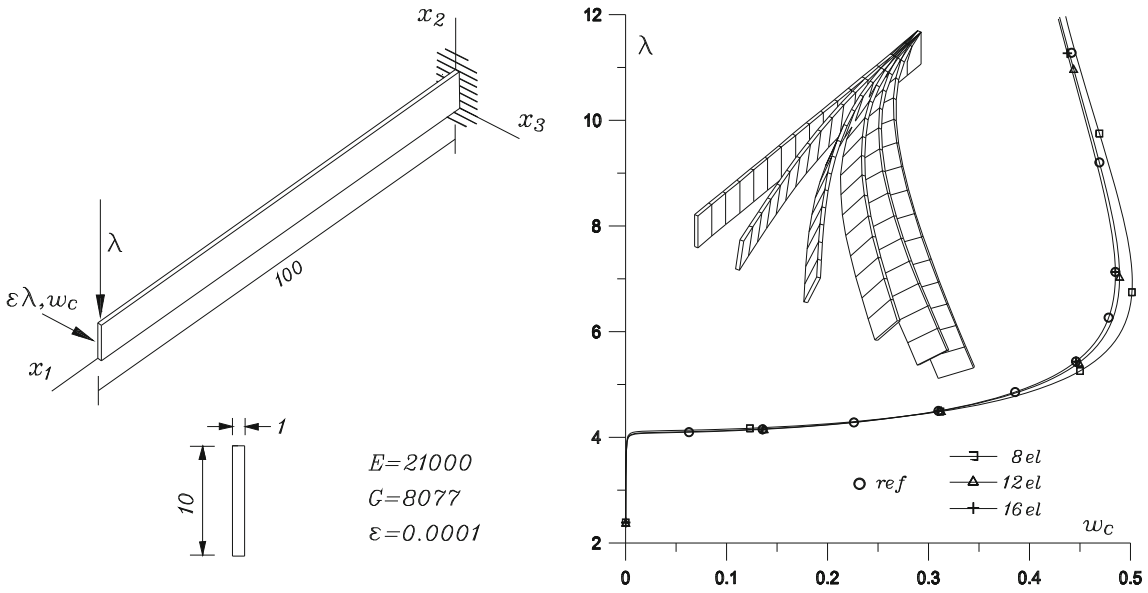

Fig. 3 Example 1: problem definition; equilibrium paths and deformed configurations for N_e=12

Table 1 Example 1: computational characteristics for the A and S based parametrization algorithms

N_e	8			12			16		
$\bar{N}^{it}_{\lambda_{(1)}}$	$4_{0.8}$	$5_{1.0}$	$6_{1.0}$	$4_{0.8}$	$5_{1.0}$	$6_{1.0}$	$4_{0.8}$	$5_{1.0}$	$6_{1.0}$
A_1-parametrization									
Second order approximation									
Steps	273	79		261	74		259	73	
N_m	3.960	4.633		3.958	4.622		3.961	4.616	
t	0.906	0.281		1.235	0.390		1.468	0.499	
Fourth order approximation									
Steps	273	80	44	261	74	43	259	73	42
N_m	3.960	4.650	4.773	3.958	4.622	4.767	3.961	4.616	4.762
t	0.999	0.359	0.203	1.297	0.438	0.281	1.687	0.546	0.328
Exact representation									
Steps	273	80	44	261	76	43	259	74	42
N_m	3.960	4.638	4.795	3.958	4.618	4.767	3.958	4.622	4.738
t	1.295	0.491	0.281	1.738	0.606	0.374	2.263	0.770	0.481
A_2-parametrization									
Second order approximation									
Steps	273	79		261	74		259	73	
N_m	3.960	4.633		3.958	4.622		3.961	4.616	
t	0.843	0.266		1.156	0.375		1.437	0.468	
Fourth order approximation									
Steps	273	80	43	261	66	43	259	65	38
N_m	3.960	4.650	4.744	3.958	4.561	4.814	3.961	4.554	4.957
t	0.937	0.296	0.187	1.250	0.385	0.265	1.640	0.471	0.274
Exact representation									
Steps	273	80	43	261	66	43	259	65	43
N_m	3.960	4.650	4.744	3.958	4.561	4.767	3.961	4.554	4.767
t	1.203	0.421	0.250	1.562	0.484	0.343	2.031	0.640	0.437
S-parametrization									
Second order approximation									
Steps	278	72		262	73		259	68	
N_m	3.964	4.625		3.962	4.644		3.961	4.603	
t	0.718	0.218		0.984	0.328		1.235	0.390	
Fourth order approximation									
Steps	280	80	41	263	72	40	260	70	39
N_m	3.964	4.671	4.854	3.962	4.654	4.825	3.962	4.649	4.795
t	0.823	0.265	0.140	1.093	0.371	0.218	1.422	0.451	0.246
Exact representation									
Steps	280	79	41	263	74	40	260	72	39
N_m	3.964	4.671	4.854	3.962	4.654	4.825	3.962	4.649	4.795
t	1.031	0.328	0.156	1.328	0.438	0.250	1.781	0.557	0.344

Based on the above definitions and by referring to the $\overset{o}{\mathbf{g}}_i = \mathbf{g}_i(0)$ definitions, local rotations and director components are now linked by the vectorial operations

$$\begin{aligned}
\mathbf{g}_1(\xi_1) &= \overset{o}{\mathbf{g}}_1 + \tilde{\varphi}_2(\xi_1)\overset{o}{\mathbf{g}}_2 - \tilde{\varphi}_3(\xi_1)\overset{o}{\mathbf{g}}_3,\\
\mathbf{g}_2(\xi_1) &= -\tilde{\varphi}_2(\xi_1)\overset{o}{\mathbf{g}}_1 + \overset{o}{\mathbf{g}}_2 + \tilde{\varphi}_1(\xi_1)\overset{o}{\mathbf{g}}_3,\\
\mathbf{g}_3(\xi_1) &= \tilde{\varphi}_3(\xi)\overset{o}{\mathbf{g}}_1 - \tilde{\varphi}_1(\xi_1)\overset{o}{\mathbf{g}}_2 + \overset{o}{\mathbf{g}}_3. \qquad (22)
\end{aligned}$$

We note that the first order accuracy of the (22) representations leads to local evaluations consistent with the small strains hypotheses. By evaluating (22) relations for $\xi_1 = -h_1/2$ and $\xi_1 = h_1/2$, respectively in the n and m nodes, we have

$$\overset{o}{\mathbf{g}}_i = (\overset{n}{\mathbf{g}}_i + \overset{m}{\mathbf{g}}_i)/2 \qquad (23)$$

and, by using orthonormality of the directors,

$$\begin{aligned}
\theta &= (\overset{n}{\mathbf{g}}_3 \cdot \overset{m}{\mathbf{g}}_2 - \overset{n}{\mathbf{g}}_2 \cdot \overset{m}{\mathbf{g}}_3)/2h_1,\\
\chi_2 &= -(\overset{n}{\mathbf{g}}_2 \cdot \overset{m}{\mathbf{g}}_1 - \overset{n}{\mathbf{g}}_1 \cdot \overset{m}{\mathbf{g}}_2)/2h_1,\\
\chi_3 &= (\overset{n}{\mathbf{g}}_3 \cdot \overset{m}{\mathbf{g}}_1 - \overset{n}{\mathbf{g}}_1 \cdot \overset{m}{\mathbf{g}}_3)/2h_1. \qquad (24)
\end{aligned}$$

Furthermore, by defining $\overset{o}{u}_i = u_i(0)$ we now obtain rigid and deformation components in the initial frame of reference by

$$\bar{u}_i(\xi_1) = \overset{o}{u}_i + \xi_1(\overset{o}{g}_{i1} - \hat{g}_{i1}) \qquad (25)$$

Table 2 Example 1: no imperfection case: normalized buckling loads for increasing aspect ratio values obtained by exact *S*-representation

J_3/J_2	γ_b		
	N_e=8	N_e=16	N_e=32
0.0002	0.9951	0.9985	0.9994
0.05	0.9225	0.9252	0.9259
0.1	0.8441	0.8459	0.8463
0.15	0.7574	0.7580	0.7581
0.2	0.6603	0.6592	0.6590
0.25	0.5498	0.5462	0.5454
0.3	0.4200	0.4122	0.4102
0.33	0.3270	0.3137	0.3102
0.35	0.2533	0.2309	0.2244
0.36	0.2102	0.1760	0.1641
0.365	0.1863	0.1394	0.1162
0.367	0.1763	0.1210	0.07677
0.3675	0.1737	0.1159	0.001505

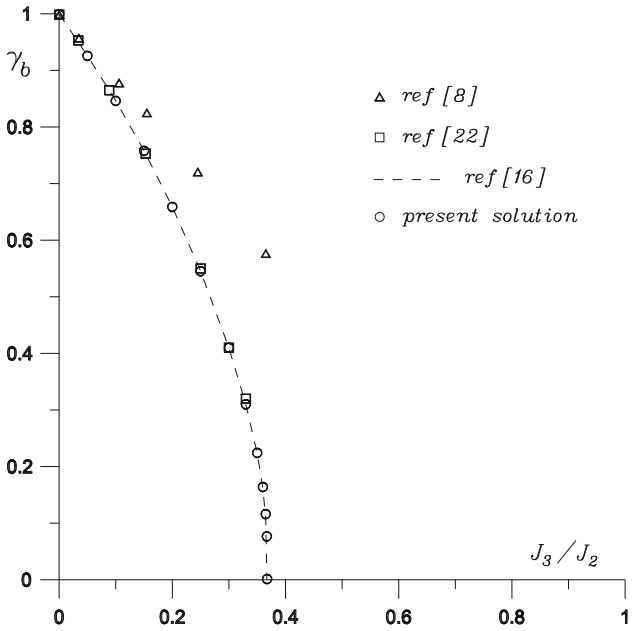

Fig. 4 Example 1, no imperfection case: normalized buckling loads versus cross section aspect ratio

and

$$\tilde{u}_i(\xi_1) = \xi_1(\varepsilon \overset{o}{g}_{1i} + \gamma_2 \overset{o}{g}_{2i} + \gamma_3 \overset{o}{g}_{3i}), \tag{26}$$

respectively. Then, in the vectorial notation, the motion of the ξ_1 point is described as

$$\mathbf{u} = \overset{o}{\mathbf{u}} + \xi_1(\overset{o}{\mathbf{g}}_1 - \hat{\mathbf{g}}_1) + \xi_1(\varepsilon \overset{o}{\mathbf{g}}_1 + \gamma_2 \overset{o}{\mathbf{g}}_2 + \gamma_3 \overset{o}{\mathbf{g}}_3). \tag{27}$$

Also here, by evaluating relation (27) for nodal coordinates $\xi_1 = -h_1/2$, $\xi_1 = h_1/2$, and by using orthonormality of the directors, we deduce that

$$\overset{o}{\mathbf{u}} = (\overset{n}{\mathbf{u}} + \overset{m}{\mathbf{u}})/2 \tag{28}$$

is the central point displacement and

$$\begin{aligned} \varepsilon &= [\overset{o}{\mathbf{g}}_1 \cdot (\overset{m}{\mathbf{u}} - \overset{n}{\mathbf{u}}) - h_1 + h_1 \overset{o}{g}_{11}]/h_1, \\ \gamma_2 &= [\overset{o}{\mathbf{g}}_2 \cdot (\overset{m}{\mathbf{u}} - \overset{n}{\mathbf{u}}) + h_1 \overset{o}{g}_{21}]/h_1, \\ \gamma_3 &= [\overset{o}{\mathbf{g}}_3 \cdot (\overset{m}{\mathbf{u}} - \overset{n}{\mathbf{u}}) + h_1 \overset{o}{g}_{31}]/h_1, \end{aligned} \tag{29}$$

are the expressions of the axial and shear deformations as a function of nodal displacement and director components.

As can be seen, n and m nodal components of displacement vector $\mathbf{u}$ and director vectors $\mathbf{g}_i$ completely define the kinematics of the beam element. In particular, the (20) and (21) linearized deformations are defined by expressions (24) and (29) while the (27) nonlinear motion of the centerline is described by the displacement vector $\overset{o}{\mathbf{u}}$ in (28) and the director vectors $\overset{o}{\mathbf{g}}_i$ in (23).

For the evaluation of the energetic quantities of the beam element, we consider the referential coordinates (ξ_i) in the element. We denote with $\mathbf{u}_P(\xi_j) = \{u_{Pi}(\xi_j)\}$ the displacement of the generic point P in the element represented in the global reference frame. Then we can refer respectively to the expression

$$\bar{\mathbf{u}}_P = \overset{o}{\mathbf{u}} + \xi_1(\overset{o}{\mathbf{g}}_1 - \hat{\mathbf{g}}_1) + \xi_2(\overset{o}{\mathbf{g}}_2 - \hat{\mathbf{g}}_2) + \xi_3(\overset{o}{\mathbf{g}}_3 - \hat{\mathbf{g}}_3) \tag{30}$$

for the rigid and to expression

$$\begin{aligned} \tilde{\mathbf{u}}_P = {} & \tilde{u}_1 \overset{o}{\mathbf{g}}_1 + \tilde{u}_2 \overset{o}{\mathbf{g}}_2 + \tilde{u}_3 \overset{o}{\mathbf{g}}_3 + (\tilde{\varphi}_3 \xi_2 - \tilde{\varphi}_2 \xi_3) \overset{o}{\mathbf{g}}_1 \\ & + \tilde{\varphi}_1(\xi_2 \overset{o}{\mathbf{g}}_3 - \xi_3 \overset{o}{\mathbf{g}}_2) \end{aligned} \tag{31}$$

for the deformation components of the motion $\mathbf{u}_P = \bar{\mathbf{u}}_P + \tilde{\mathbf{u}}_P$.

In the hypotheses of elastic materials, the energetic quantities involved are the internal and external energy

$$U = \frac{1}{2} \int_V \boldsymbol{\varepsilon}_P : \boldsymbol{\sigma}_P dV, \qquad W = \int_V \mathbf{p} \cdot \mathbf{u}_P dV, \tag{32}$$

respectively. In (32) we denote with V the volume of beam element, $\mathbf{p}$ the vector of external loads while $\boldsymbol{\varepsilon}_P$ and $\boldsymbol{\sigma}_P$ are the infinitesimal strain and stress tensors in the body, respectively.

The estimation of the internal energy can be carried out by extracting the contributions due to the deformation from the $\mathbf{u}_P$ motion. Then, the projection of $\tilde{\mathbf{u}}_P$ in (31) in the $\overset{o}{\mathbf{g}}_i$ directions gives the infinitesimal displacements:

$$\begin{aligned} \tilde{u} &= \tilde{\mathbf{u}}_P \cdot \overset{o}{\mathbf{g}}_1 = \xi_1(\varepsilon + \chi_2 \xi_2 - \chi_3 \xi_3), \\ \tilde{v} &= \tilde{\mathbf{u}}_P \cdot \overset{o}{\mathbf{g}}_2 = \xi_1(\gamma_2 - \theta \xi_3), \\ \tilde{w} &= \tilde{\mathbf{u}}_P \cdot \overset{o}{\mathbf{g}}_3 = \xi_1(\gamma_3 + \theta \xi_2). \end{aligned} \tag{33}$$

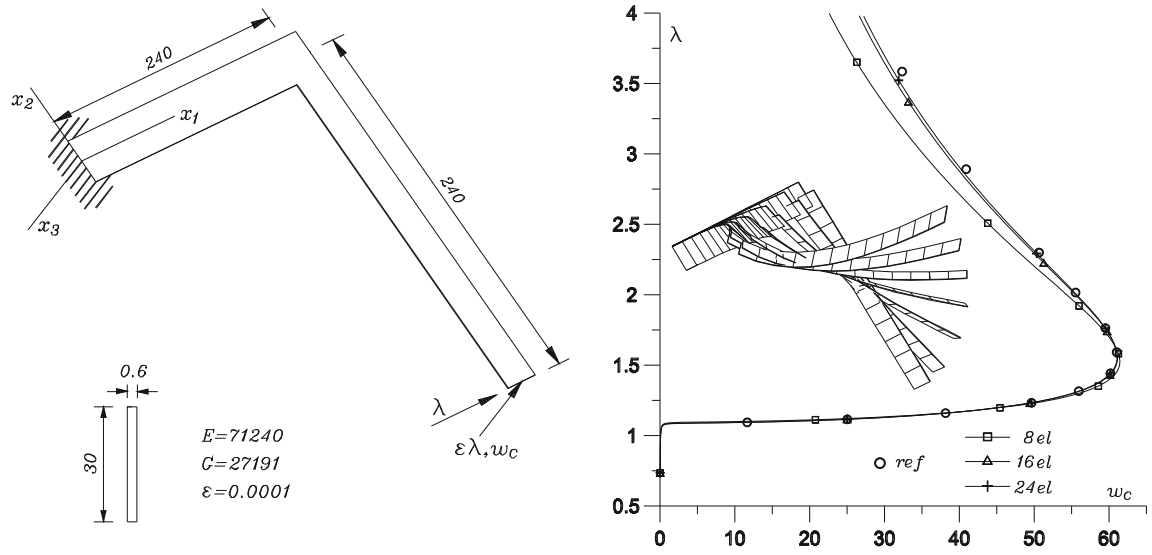

Fig. 5 Example 2: problem definition; equilibrium paths and deformed configurations for N_e=24

By using this deformation kinematics, we define the following infinitesimal strain components of the $\boldsymbol{\varepsilon}_P$ tensor:

$$\varepsilon_{11} = \varepsilon + \chi_2\xi_2 - \chi_3\xi_3, \quad \varepsilon_{12} = \frac{1}{2}(\gamma_2 - \omega\theta),$$
$$\varepsilon_{13} = \frac{1}{2}(\gamma_3 + \omega\theta), \tag{34}$$

and $\varepsilon_{23} = 0$. In (34) shearing contributions due to the torsional mode are modelled by a $\omega = \omega(\xi_2, \xi_3)$ function while those due to the flexural modes are omitted to overcome locking effects.

Extensional components ε_{22} and ε_{33} are then obtained by imposing the statical assumptions $\sigma_{22} = \sigma_{33} = 0$ on the $\boldsymbol{\sigma}_P$ stress tensor. Then we have

$$\varepsilon_{22} = \varepsilon_{33} = -\frac{\lambda}{2(\lambda+\mu)}\varepsilon_{11}, \tag{35}$$

where λ and μ are the Lamé coefficients. By using the expressions (35), the remaining stress components are:

$$\sigma_{11} = 2\mu\varepsilon_{11} + \lambda(\varepsilon_{11} + \varepsilon_{22} + \varepsilon_{33}) = \frac{2\mu+3\lambda}{\lambda+\mu}\mu\varepsilon_{11} = E\varepsilon_{11},$$
$$\sigma_{12} = 2\mu\varepsilon_{12} = 2G\varepsilon_{12},$$
$$\sigma_{13} = 2\mu\varepsilon_{13} = 2G\varepsilon_{13} \tag{36}$$

and $\sigma_{23} = 0$. In (36), E and G are the Young and shear moduli, respectively.

By integrating the internal energy contribution over the section area we have:

$$\int_A \boldsymbol{\varepsilon}_P : \boldsymbol{\sigma}_P dA = \int_A (E\varepsilon_{11}^2 + 4G\varepsilon_{12}^2 + 4G\varepsilon_{13}^2) dA$$
$$= E(A\varepsilon^2 + J_3\chi_2^2 + J_2\chi_3^2)$$
$$+G[A(\gamma_2^2 + \gamma_3^2) + 2\theta^2 \int_A \omega^2 dA$$
$$+2(\gamma_3 - \gamma_2)\theta \int_A \omega dA], \tag{37}$$

where J_2 and J_3 are the second moments of area about the related principal axes. Besides, by assuming $\int_A \omega dA = 0$ and $J_\omega = 2\int_A \omega^2 dA$ is the St-Venant torsion constant, we can write:

$$U = \frac{1}{2}\int_{-h_1/2}^{h_1/2}\int_A \boldsymbol{\varepsilon}_P : \boldsymbol{\sigma}_P dA$$
$$= \frac{1}{2}h_1[E(A\varepsilon^2 + J_3\chi_2^2 + J_2\chi_3^2)$$
$$+G(A\gamma_2^2 + A\gamma_3^2 + J_\omega\theta^2)]. \tag{38}$$

Note that coupling axial-torsional terms and the warping effect of the cross-section are not taken into account. In effect, here the tests are carried out to prove the computational effectiveness of the finite rotations treatment. Better models for taking into account the torsional effects in the beam, however, can also be considered (Mohri et al. [29,30], can be referred to for details of this).

External work W is defined in (32) by the (30) and (31) expressions of the displacement vector. Note that as the kinematics of the element being modelled as a 3D body, only external forces must be assigned.

Table 3 Example 2: computational characteristics for the A and S based parametrization algorithms

N_e	8			16			24		
$\bar{N}^{it}_{\lambda_{(1)}}$	$4_{0.20}$	$5_{0.25}$	$6_{0.25}$	$4_{0.20}$	$5_{0.25}$	$6_{0.25}$	$4_{0.20}$	$5_{0.25}$	$6_{0.25}$
A_1-parametrization									
	Second order approximation								
Steps	545	158		508	146		548	149	
N_m	3.980	4.861		3.978	4.870		3.980	4.846	
t	1.688	0.562		2.859	1.046		4.531	1.562	
	Fourth order approximation								
Steps	545	158	88	508	147	87	548	147	80
N_m	3.980	4.861	5.295	3.978	4.871	5.218	3.980	4.871	5.412
t	1.937	0.671	0.422	3.312	1.171	0.750	5.218	1.703	1.015
	Exact representation								
Steps	545	158	88	494	147	83	548	147	79
N_m	3.980	4.861	5.273	3.977	4.871	5.361	3.980	4.871	5.418
t	2.526	0.998	0.573	4.223	1.558	1.051	6.775	2.247	1.345
A_2-parametrization									
	Second order approximation								
Steps	545	158		507	146		548	149	
N_m	3.980	4.861		3.978	4.870		3.980	4.853	
t	1.640	0.532		2.794	1.010		4.484	1.453	
	Fourth order approximation								
Steps	545	159	89	508	147	87	548	146	79
N_m	3.980	4.862	5.303	3.978	4.871	5.310	3.980	4.870	5.506
t	1.828	0.596	0.406	3.009	1.156	0.718	5.078	1.656	0.909
	Exact representation								
Steps	545	159	89	508	147	87	548	146	79
N_m	3.980	4.862	5.303	3.978	4.871	5.310	3.980	4.870	5.506
t	2.312	0.828	0.516	3.968	1.453	0.921	6.250	2.078	1.296
S-parametrization									
	Second order approximation								
Steps	489	161		456	158		454	167	
N_m	3.978	4.888		3.976	4.886		3.976	4.802	
t	1.281	0.484		2.187	0.921		3.156	1.390	
	Fourth order approximation								
Steps	495	166	87	460	161	84	459	160	85
N_m	3.978	4.861	5.138	3.976	4.857	5.333	3.976	4.894	5.202
t	1.437	0.558	0.312	2.515	1.063	0.640	3.625	1.526	0.852
	Exact representation								
Steps	495	166	87	460	162	88	459	160	92
N_m	3.978	4.861	5.138	3.976	4.858	5.307	3.976	4.894	5.155
t	1.796	0.750	0.391	3.078	1.312	0.766	4.531	1.921	1.119

5 Variational formulation and linearization

In this section, we summarize the derivation of the used variational formulation and related consistent linearization. This is done mainly to facilitate understanding the derivation of the stiffness matrix. Although a multiplicative approach is here exploited, also the necessary linear transformation to define additive representation is established. For detailed expositions, the reader is referred to the relevant cited literature.

We denote respectively by $\boldsymbol{\varepsilon}^T = \{\varepsilon, \gamma_2, \gamma_3\}$ and $\boldsymbol{\theta}^T = \{\theta, \chi_2, \chi_3\}$ the deformation and the curvature vector while, if not specified, quantities refer to the central point of the

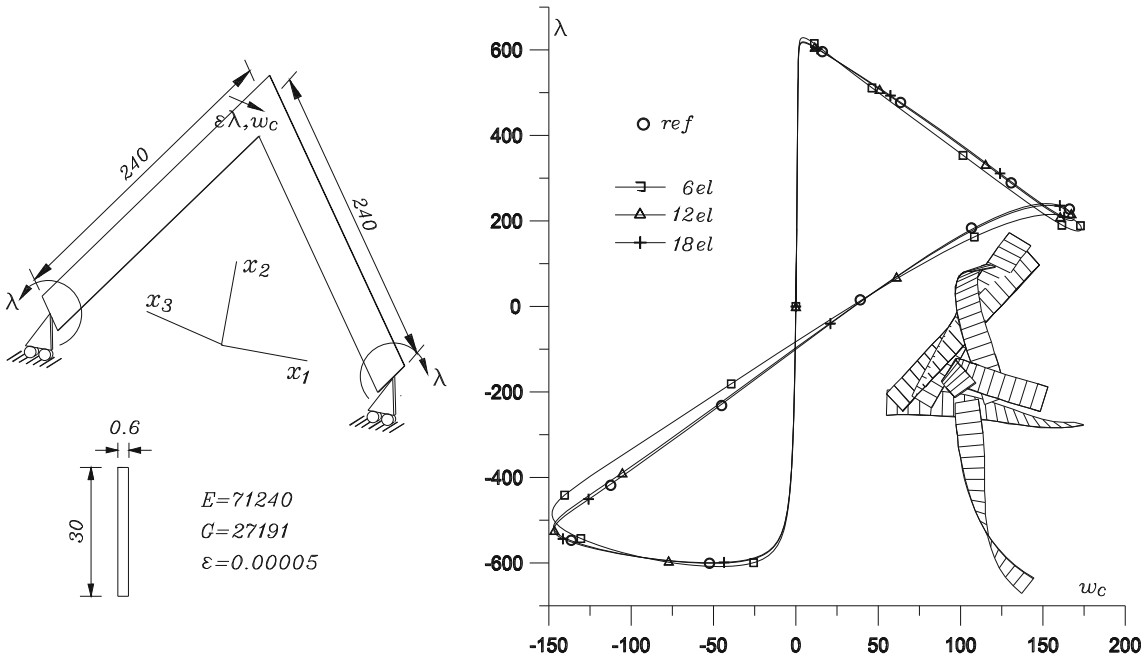

Fig. 6 Example 3: problem definition; equilibrium paths and deformed configurations for N_e=18

element. By defining the $dv = (\overset{m}{v} - \overset{n}{v})/h_1$ discrete counterpart of the derivative of v with respect to the reference coordinate ξ_1, from the (29) expressions we have

$$\boldsymbol{\varepsilon} = \mathbf{G}^T d\mathbf{u} + \mathbf{G}^T \mathbf{k}_1 - \mathbf{k}_1 = \mathbf{G}^T d\mathbf{x} - \mathbf{k}_1, \tag{39}$$

where $\mathbf{x}$ is the position vector of the centroid point. By indicating with $\mathbf{v}_\times$ the skew-symmetric matrix formed by the component of $\mathbf{v}$, from the (22) vectorial operation we can write $\overset{m}{\mathbf{G}} = \mathbf{G}(\mathbf{I} + \overset{m}{\tilde{\boldsymbol{\varphi}}}_\times)$ and $\overset{n}{\mathbf{G}} = \mathbf{G}(\mathbf{I} + \overset{n}{\tilde{\boldsymbol{\varphi}}}_\times)$, where $\tilde{\boldsymbol{\varphi}}$ is a material incremental rotation. Then, relation $d\mathbf{G} = \mathbf{G}d\tilde{\boldsymbol{\varphi}}_\times$ leads to the following expression

$$\boldsymbol{\theta}_\times = d\tilde{\boldsymbol{\varphi}}_\times = \mathbf{G}^T d\mathbf{G}. \tag{40}$$

As we can see, the classical definitions of material deformation and curvature are obtained in (39) and (40), respectively.

Because rotation operator belongs to the Lie group of proper orthogonal linear transformations $SO(3) = \{\mathbf{G} : \mathcal{R}^3 \to \mathcal{R}^3 \mid \mathbf{G}^T\mathbf{G} = \mathbf{I}, \det\mathbf{G} = +1\}$, admissible variations are to performed by

$$\delta\mathbf{G} = \delta\boldsymbol{\varphi}_\times \mathbf{G}, \tag{41}$$

where $\delta\boldsymbol{\varphi}$ is the spatial component of the angular variation. Then, by (39) we have

$$\delta\boldsymbol{\varepsilon} = (\delta\boldsymbol{\varphi}_\times \mathbf{G})^T d\mathbf{x} + \mathbf{G}^T d\delta\mathbf{x} = \mathbf{G}^T(d\delta\mathbf{x} + d\mathbf{x}_\times \delta\boldsymbol{\varphi}), \tag{42}$$

while (40) implies

$$\begin{aligned}\delta\boldsymbol{\theta}_\times &= (\delta\boldsymbol{\varphi}_\times \mathbf{G})^T d\mathbf{G} + \mathbf{G}^T d\delta\mathbf{G} \\ &= \mathbf{G}^T \delta\boldsymbol{\varphi}_\times^T d\mathbf{G} + \mathbf{G}^T[d\delta\boldsymbol{\varphi}_\times \mathbf{G} + \delta\boldsymbol{\varphi}_\times d\mathbf{G}] \\ &= \mathbf{G}^T d\delta\boldsymbol{\varphi}_\times \mathbf{G},\end{aligned} \tag{43}$$

and therefore

$$\delta\boldsymbol{\theta} = \mathbf{G}^T d\delta\boldsymbol{\varphi}. \tag{44}$$

In the previous calculations, classical vectorial relations and transformations between spatial and material descriptions have been used. We note that, by Eqs. (42) and (44), variations of the given deformation and curvature vectors in terms of spatial angular variation follow the conventional definitions. If $\mathbf{n}$ and $\mathbf{m}$ respectively denote the internal stress resultants energy conjugated to the $\delta\boldsymbol{\varepsilon}$ and $\delta\boldsymbol{\theta}$ virtual strain measures, the expression for the internal virtual work is written as

$$\delta U = h_1[\mathbf{n}^T \delta\boldsymbol{\varepsilon} + \mathbf{m}^T \delta\boldsymbol{\theta}]. \tag{45}$$

We note that (42) and (44) definitions use $\boldsymbol{\varphi}$ as primary variable to describe rotations and $\delta U = \mathbf{f}(\mathbf{x}, \mathbf{G})^T \{d\delta\mathbf{x}, \delta\boldsymbol{\varphi}*, d\delta\boldsymbol{\varphi}\}$ results, where $\mathbf{f}$ is the internal force vector. By referring to the $\mathbf{G} = \mathbf{R}\bar{\mathbf{R}}$ composition of rotation operators, above expressions are consistent when the multiplicative representation

$$\mathbf{R}^{(k+1)} = \exp(\Delta\boldsymbol{\varphi}_\times^{(k)})\mathbf{R}^{(k)}, \qquad \boldsymbol{\varphi}^{(k+1)} = R^{-1}(\mathbf{R}^{(k+1)}) \tag{46}$$

is used in relation to the $\Delta\boldsymbol{\varphi}$ incremental rotation. The (46) update procedure must be performed for each iterative step k of the solution process. In effect, at the converged point

Table 4 Example 3: computational characteristics for the A and S based parametrization algorithms

N_e	6			12			18		
$\bar{N}^{it}_{\lambda_{(1)}}$	4_{50}	5_{70}	6_{90}	4_{50}	5_{70}	6_{90}	4_{50}	5_{70}	6_{90}
A_1-parametrization									
	Second order approximation								
Steps	1081	327		949	350		998	356	
N_m	3.998	4.936		3.997	4.926		3.998	4.902	
t	2.688	1.000		4.188	1.875		6.375	2.781	
	Fourth order approximation								
Steps	1106	329	186	952	321	202	1024	345	235
N_m	3.996	4.936	5.608	3.993	4.935	5.703	3.995	4.916	5.434
t	2.894	1.125	0.687	4.843	1.968	1.484	8.613	3.140	2.328
	Exact representation								
Steps	1076	329	181	1017	345	217	998	362	228
N_m	3.999	4.936	5.669	3.999	4.936	5.548	3.999	4.906	5.482
t	4.002	1.541	0.951	6.726	2.838	1.984	9.564	5.151	2.969
A_2-parametrization									
	Second order approximation								
Steps	1081	327		949	350		998	354	
N_m	3.998	4.936		3.997	4.926		3.998	4.938	
t	2.578	0.953		4.115	1.806		6.257	2.745	
	Fourth order approximation								
Steps	1036	313	181	952	341	210	998	364	239
N_m	3.999	4.936	5.696	3.993	4.962	5.529	3.998	4.893	5.406
t	2.765	1.015	0.631	4.750	2.078	1.406	7.109	3.094	2.265
	Exact representation								
Steps	1036	313	181	952	341	210	998	374	234
N_m	3.999	4.936	5.696	3.993	4.962	5.529	3.998	4.893	5.466
t	3.500	1.312	0.890	5.766	2.562	1.781	8.781	4.016	2.812
S-parametrization									
	Second order approximation								
Steps	1014	373		1009	395		1027	388	
N_m	4.000	4.917		3.997	4.896		3.998	4.938	
t	2.171	0.884		3.843	1.746		5.609	2.546	
	Fourth order approximation								
Steps	1023	364	231	1010	372	255	1028	375	265
N_m	3.999	4.931	5.466	3.998	4.907	5.298	3.998	4.935	5.254
t	2.437	0.977	0.596	4.313	1.905	1.262	6.313	2.875	2.090
	Exact representation								
Steps	1023	362	243	1010	375	258	1028	385	274
N_m	3.999	4.931	5.440	3.998	4.907	5.469	3.998	4.935	5.255
t	3.015	1.296	0.874	5.375	2.431	1.739	7.921	3.637	2.738

$\Delta\boldsymbol{\varphi} \to \mathbf{0}$, $\Delta\mathbf{R} = \exp(\Delta\boldsymbol{\varphi}_\times) \to \mathbf{I}$ results and variation of the (46) representation agrees with the consistent variation (41). The kind of representation used to define the $\Delta\mathbf{R}$ operator may influence only the convergence behaviour of the iterative scheme. When an expression

$$\delta\boldsymbol{\varphi} = \mathbf{A}(\boldsymbol{\psi})\delta\boldsymbol{\psi} \tag{47}$$

between $\delta\boldsymbol{\varphi}$ angular and $\delta\boldsymbol{\psi}$ rotation vector variations consistent with the (41) relation is given, the different form of the material virtual strains

$$\delta\boldsymbol{\varepsilon} = \mathbf{G}^T(d\delta\mathbf{x} + d\mathbf{x}_\times\mathbf{A}(\boldsymbol{\psi})\delta\boldsymbol{\psi}), \quad \delta\boldsymbol{\theta} = \mathbf{G}^T d[\mathbf{A}(\boldsymbol{\psi})\delta\boldsymbol{\psi}] \tag{48}$$

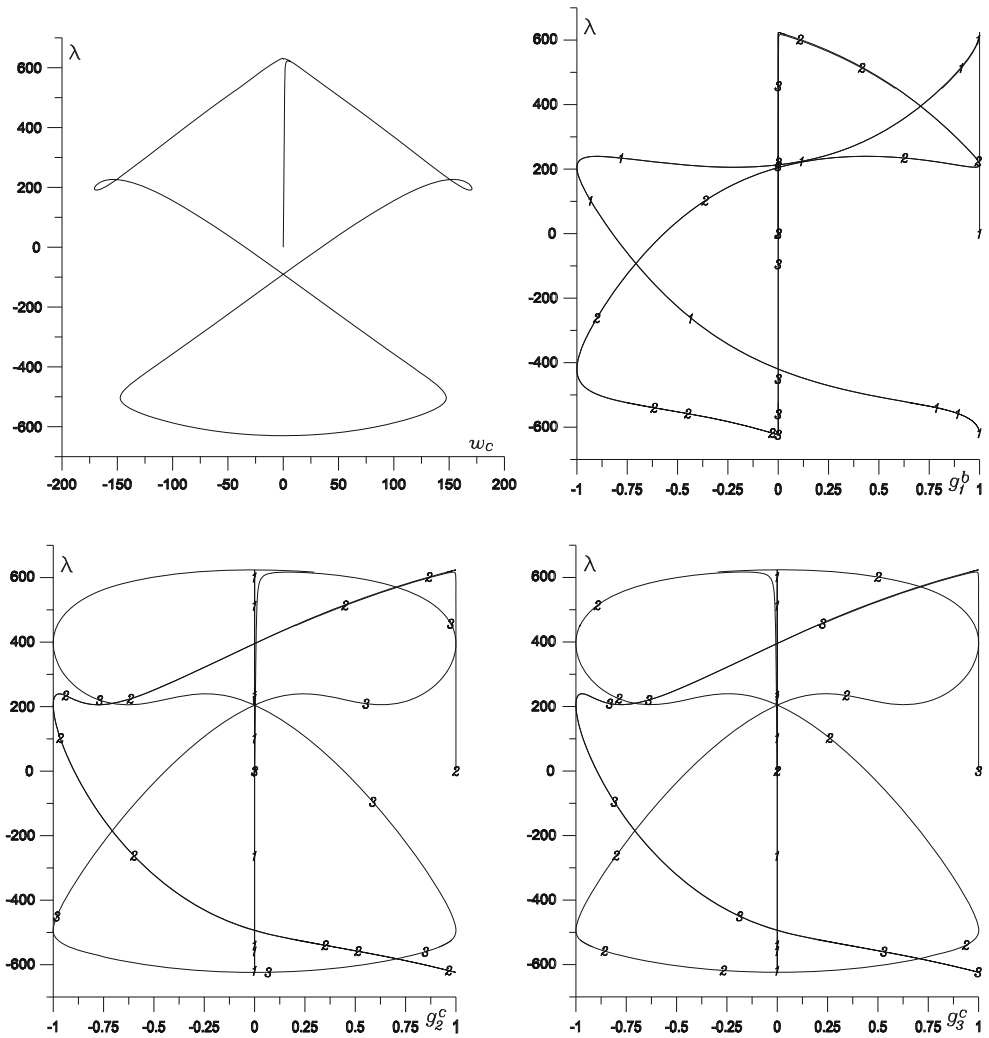

Fig. 7 Example 3: equilibrium path and director component values for the first and second revolution

is used. Expressions (48) are now connected with the additive representation

$$\boldsymbol{\psi}^{(k+1)} = \boldsymbol{\psi}^{(k)} + \Delta\boldsymbol{\psi}^{(k)}, \quad \mathbf{R}^{(k+1)} = \exp(\boldsymbol{\psi}_{\times}^{(k+1)}) \tag{49}$$

where $\Delta\boldsymbol{\psi}$ is the incremental rotation vector. Essentially, by the (47) relation the configuration space is simplified to a linear vector space. The $\boldsymbol{\psi}$ rotation vector is used as primary variable while $\delta U = \mathbf{f}(\mathbf{x}, \boldsymbol{\psi})^T \{d\delta\mathbf{x}, \delta\boldsymbol{\psi}, d\delta\boldsymbol{\psi}\}$ is the form of the internal virtual work.

We use now the symbol d_α to denote operator $d/d\alpha\ |_{\alpha=0}$. In the multiplicative approach the consistent linearization of the virtual work leads to

$$Lin(\mathbf{f}) = \mathbf{f} + d_\alpha \mathbf{f}\left[\exp(\alpha\Delta\boldsymbol{\varphi}_{\times})\mathbf{G}, \mathbf{x} + \alpha\Delta\mathbf{x}\right] \tag{50}$$

while, in the additive approach, we have

$$Lin(\mathbf{f}) = \mathbf{f} + d_\alpha \mathbf{f}\left(\boldsymbol{\psi} + \alpha\Delta\boldsymbol{\psi}, \mathbf{x} + \alpha\Delta\mathbf{x}\right). \tag{51}$$

The tangent stiffness matrix related to the (50) linearization is unsymmetric although inexpensive calculations are required to compute its coefficients. In contrast, the (51) linearization provides symmetric but very complex tangent stiffness matrices. In effect, seconde derivative of the $\mathbf{A}(\boldsymbol{\psi})$ operator is involved in the linerization process which would be extremely complicated to calculate. Additionally, we remark that simplifications can be operated on the (51) linearization in the additive approach. In such cases, the continuation method with the resulting approximate tangent stiffness matrix has not difficulties in computing the equilibrium points. However, exact values of the tangent stiffness are required for locating the bifurcation points on the equilibrium path.

We now discuss of the used S parametrization in the multiplicative approach. By referring to the $\mathbf{G} = \mathbf{E}\bar{\mathbf{E}}$ composition, let components $r_1 = -e_{32}$, $r_2 = e_{31}$ and $r_3 = -e_{21}$ of $\mathbf{r}$ be the three rotation parameters retained to describe the rotation

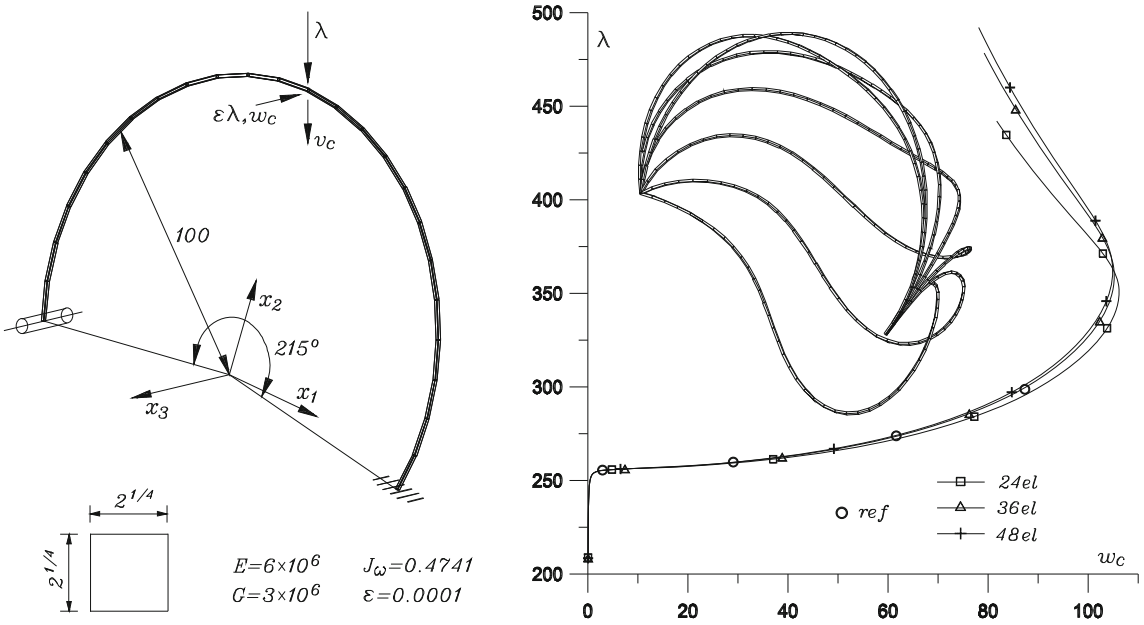

Fig. 8 Example 4: problem definition; equilibrium paths and deformed configurations for N_e=48

operator $\mathbf{E}$. Here the multiplicative representation assumes the form

$$\begin{aligned}\mathbf{E}^{(k+1)} &= \Delta\mathbf{E}^{(k)}\mathbf{E}^{(k)},\\ \mathbf{r}^{(k+1)^T} &= \left\{-E_{23}^{(k+1)}, E_{13}^{(k+1)}, -E_{12}^{(k+1)}, \right\}\end{aligned} \tag{52}$$

in relation to the $\Delta\mathbf{r}$ incremental rotation vector. As said above, the representation used to define the incremental rotation operator may influence only the convergence behaviour of the iterative scheme. The main requirement is that, at the solution point $\Delta\mathbf{r} \to \mathbf{0}$, variation of the (52) representation agrees with the consistent variation (41), as $\delta\mathbf{E} = d_\alpha\mathbf{E}(\mathbf{0}+\alpha\delta\mathbf{r}) = \delta\mathbf{r}_\times\mathbf{E}$ verifies. The linearization of the virtual work leads now to

$$\begin{aligned}&\{d\delta\mathbf{u}, \delta\mathbf{r}, d\delta\mathbf{r}\}^T d_\alpha\mathbf{f}\big[\mathbf{E}(\alpha\Delta\mathbf{r})\mathbf{G}, \mathbf{u}+\alpha\Delta\mathbf{u}\big]\\ &\quad= \{d\delta\mathbf{u}, \delta\mathbf{r}, d\delta\mathbf{r}\}^T\mathbf{K}\{d\Delta\mathbf{u}, \Delta\mathbf{r}, d\Delta\mathbf{r}\}\\ &\quad= h_1\left[d_\alpha\mathbf{n}_\Delta^T\delta\boldsymbol{\varepsilon} + d_\alpha\mathbf{m}_\Delta^T\delta\boldsymbol{\theta}\right]\\ &\qquad+h_1\left[\mathbf{n}^T d_\alpha\delta\boldsymbol{\varepsilon}_\Delta + \mathbf{m}^T d_\alpha\delta\boldsymbol{\theta}_\Delta\right],\end{aligned} \tag{53}$$

where $\mathbf{K}$ is the tangent stiffness matrix and subscript Δ denotes perturbation $V_\Delta(v+\alpha\Delta v)$. The first and second terms in (53) define the material $\mathbf{K}^m$ and geometric $\mathbf{K}^g$ stiffness matrix, respectively.

Defining the material stiffness $\mathbf{C}_\varepsilon$ and $\mathbf{C}_\theta$ respectively by $\mathbf{C}_\varepsilon = \mathrm{Diag}(EA, GA, GA)$ and $\mathbf{C}_\theta = \mathrm{Diag}(GJ_\omega, EJ_2, EJ_3)$, we can write directly

$$d_\alpha\mathbf{n}_\Delta = \mathbf{C}_\varepsilon d_\alpha\boldsymbol{\varepsilon}_\Delta = \mathbf{C}_\varepsilon\mathbf{G}^T(d\Delta\mathbf{u} + d\mathbf{u}_\times\Delta\mathbf{r}), \tag{54}$$

and

$$d_\alpha\mathbf{m}_\Delta = \mathbf{C}_\theta d_\alpha\boldsymbol{\theta}_\Delta = \mathbf{C}_\theta\mathbf{G}^T d\Delta\mathbf{r}. \tag{55}$$

Then, the material stiffness matrix is symmetric with coefficients defined by

$$\begin{aligned}&\mathbf{K}^m_{d\delta\mathbf{u},d\Delta\mathbf{u}} = \mathbf{G}\mathbf{C}_\varepsilon\mathbf{G}^T, \quad \mathbf{K}^m_{d\delta\mathbf{u},\Delta\mathbf{r}} = \mathbf{G}\mathbf{C}_\varepsilon\mathbf{G}^T d\mathbf{u}_\times, \quad \mathbf{K}^m_{d\delta\mathbf{u},d\Delta\mathbf{r}} = 0,\\ &\mathbf{K}^m_{\delta\mathbf{r},d\Delta\mathbf{u}} = d\mathbf{u}_\times^T\mathbf{G}\mathbf{C}_\varepsilon\mathbf{G}^T, \quad \mathbf{K}^m_{\delta\mathbf{r},\Delta\mathbf{r}} = d\mathbf{u}_\times^T\mathbf{G}\mathbf{C}_\varepsilon\mathbf{G}^T d\mathbf{u}_\times, \quad \mathbf{K}^m_{\delta\mathbf{r},d\Delta\mathbf{r}} = 0,\\ &\mathbf{K}^m_{d\delta\mathbf{r},d\Delta\mathbf{u}} = 0, \quad \mathbf{K}^m_{d\delta\mathbf{r},\Delta\mathbf{r}} = 0, \quad \mathbf{K}^m_{d\delta\mathbf{r},d\Delta\mathbf{r}} = \mathbf{G}\mathbf{C}_\theta\mathbf{G}^T.\end{aligned} \tag{56}$$

To calculate the geometric stiffness term we first linearize $\delta\boldsymbol{\varepsilon}$ and $\delta\boldsymbol{\theta}$ by

$$\begin{aligned}d_\alpha\delta\boldsymbol{\varepsilon}_\Delta &= d_\alpha\mathbf{G}_\Delta^T(d\delta\mathbf{u} + d\mathbf{u}_\times\delta\mathbf{r}) + \mathbf{G}^T d_\alpha\mathbf{u}_{\times\Delta}\delta\mathbf{r}\\ &= (\Delta\mathbf{r}_\times\mathbf{G})^T(d\delta\mathbf{u} + d\mathbf{u}_\times\delta\mathbf{r}) + \mathbf{G}^T d\Delta\mathbf{u}_\times\delta\mathbf{r}\end{aligned} \tag{57}$$

and

$$d_\alpha\delta\boldsymbol{\theta}_\Delta = d_\alpha\mathbf{G}_\Delta^T d\delta\mathbf{r} = (\Delta\mathbf{r}_\times\mathbf{G})^T d\delta\mathbf{r}. \tag{58}$$

By inserting (57) and (58) expressions in the geometric stiffness terms of (53), after some manipulations, we have

$$\begin{aligned}\mathbf{n}^T d_\alpha\delta\boldsymbol{\varepsilon}_\Delta &= d\delta\mathbf{u}^T(\mathbf{G}\mathbf{n})_\times^T\Delta\mathbf{r} + \delta\mathbf{r}^T d\delta\mathbf{u}_\times^T(\mathbf{G}\mathbf{n})_\times^T\Delta\mathbf{r}\\ &\quad+\delta\mathbf{r}^T(\mathbf{G}\mathbf{n})_\times d\Delta\mathbf{u}\end{aligned} \tag{59}$$

and

$$\mathbf{m}^T d_\alpha\delta\boldsymbol{\theta}_\Delta = d\delta\mathbf{r}^T(\mathbf{G}\mathbf{m})_\times^T\Delta\mathbf{r}. \tag{60}$$

Finally, the geometric stiffness matrix is unsymmetric with coefficients given by

$$\begin{aligned}&\mathbf{K}^g_{d\delta\mathbf{u},d\Delta\mathbf{u}} = 0, \mathbf{K}^g_{d\delta\mathbf{u},\Delta\mathbf{r}} = (\mathbf{G}\mathbf{n})_\times^T, \quad \mathbf{K}^g_{d\delta\mathbf{u},d\Delta\mathbf{r}} = 0,\\ &\mathbf{K}^g_{\delta\mathbf{r},d\Delta\mathbf{u}} = (\mathbf{G}\mathbf{n})_\times, \quad \mathbf{K}^g_{\delta\mathbf{r},\Delta\mathbf{r}} = d\mathbf{u}_\times^T(\mathbf{G}\mathbf{n})_\times^T, \quad \mathbf{K}^g_{\delta\mathbf{r},d\Delta\mathbf{r}} = 0,\\ &\mathbf{K}^g_{d\delta\mathbf{r},d\Delta\mathbf{u}} = 0, \quad \mathbf{K}^g_{d\delta\mathbf{r},\Delta\mathbf{r}} = (\mathbf{G}\mathbf{m})_\times^T, \quad \mathbf{K}^g_{d\delta\mathbf{r},d\Delta\mathbf{r}} = 0.\end{aligned} \tag{61}$$

Table 5 Example 4: computational characteristics for the A and S based parametrization algorithms

N_e	24			36			48		
$\bar{N}^{it}_{\lambda_{(1)}}$	4_{20}	5_{40}	6_{40}	4_{20}	5_{40}	6_{40}	4_{20}	5_{40}	6_{40}
A_1-parametrization									
	Second order approximation								
Steps	365	140		358	134		337	134	
N_m	3.962	4.614		3.964	4.604		3.976	4.604	
t	3.078	1.328		4.344	1.953		5.469	2.500	
	Fourth order approximation								
Steps	365	140	98	358	134	113	337	134	98
N_m	3.962	4.614	4.500	3.964	4.604	4.372	3.976	4.604	4.520
t	3.515	1.546	1.078	5.046	2.250	1.734	6.312	2.906	2.140
	Exact representation								
Steps	365	140	104	358	134	113	337	134	98
N_m	3.962	4.614	4.481	3.964	4.604	3.976	4.604	4.520	
t	4.510	2.050	1.492	6.545	2.887	2.296	8.137	3.789	2.739
A_2-parametrization									
	Second order approximation								
Steps	365	141		358	134		337	134	
N_m	3.962	4.617		3.964	4.604		3.976	4.604	
t	2.940	1.298		4.268	1.859		5.396	2.477	
	Fourth order approximation								
Steps	365	140	114	358	134	113	337	134	99
N_m	3.962	4.614	4.254	3.964	4.604	4.381	3.976	4.604	4.515
t	3.406	1.500	1.015	4.921	2.125	1.709	6.109	2.874	2.015
	Exact representation								
Steps	365	140	114	358	134	111	337	134	99
N_m	3.962	4.614	4.254	3.964	4.604	4.396	3.976	4.604	4.515
t	4.171	1.890	1.406	6.031	2.656	2.095	7.500	3.484	2.546
S-parametrization									
	Second order approximation								
Steps	362	152		370	149		352	138	
N_m	3.981	4.579		3.981	4.503		3.980	4.630	
t	2.563	1.209		3.781	1.712		4.765	2.203	
	Fourth order approximation								
Steps	350	148	109	372	143	106	354	140	101
N_m	3.980	4.608	4.367	3.981	4.566	4.406	3.980	4.600	4.475
t	2.765	1.343	0.969	4.375	1.922	1.359	5.469	2.515	1.781
	Exact representation								
Steps	350	148	120	370	143	112	354	140	99
N_m	3.980	4.608	4.200	3.981	4.566	4.281	3.980	4.600	4.479
t	3.484	1.718	1.275	4.859	2.359	1.782	6.843	3.125	2.193

If an additive approach is used, as said the linear transformation $\delta\boldsymbol{\varphi} = \mathbf{A}(\mathbf{r})\delta\mathbf{r}$ is to be established. From the (41) relation, this is done by imposing $d_\alpha \mathbf{G}(\mathbf{r}+\alpha\delta\mathbf{r}) = \delta\boldsymbol{\varphi}_\times \mathbf{G}(\mathbf{r})$ or, equivalently

$$d_\alpha \mathbf{E}(\mathbf{r} + \alpha\delta\mathbf{r}) = \delta\boldsymbol{\varphi}_\times \mathbf{E}(\mathbf{r}). \tag{62}$$

Because in the parametrization the E_{23}, E_{13} and E_{12} coefficients of $\mathbf{E}$ compose directly the rotation vector $\mathbf{r}$, we can write

$$d_\alpha[\mathbf{E}(\mathbf{r}+\alpha\delta\mathbf{r})]_{23} = d_\alpha(e_{32}+\alpha\delta e_{32}) = -\delta r_1 = \delta\varphi_3 e_{31} - \delta\varphi_1 e_{33},$$
$$d_\alpha[\mathbf{E}(\mathbf{r}+\alpha\delta\mathbf{r})]_{13} = d_\alpha(e_{31}+\alpha\delta e_{31}) = \delta r_2 = -\delta\varphi_3 e_{32} + \delta\varphi_2 e_{33},$$

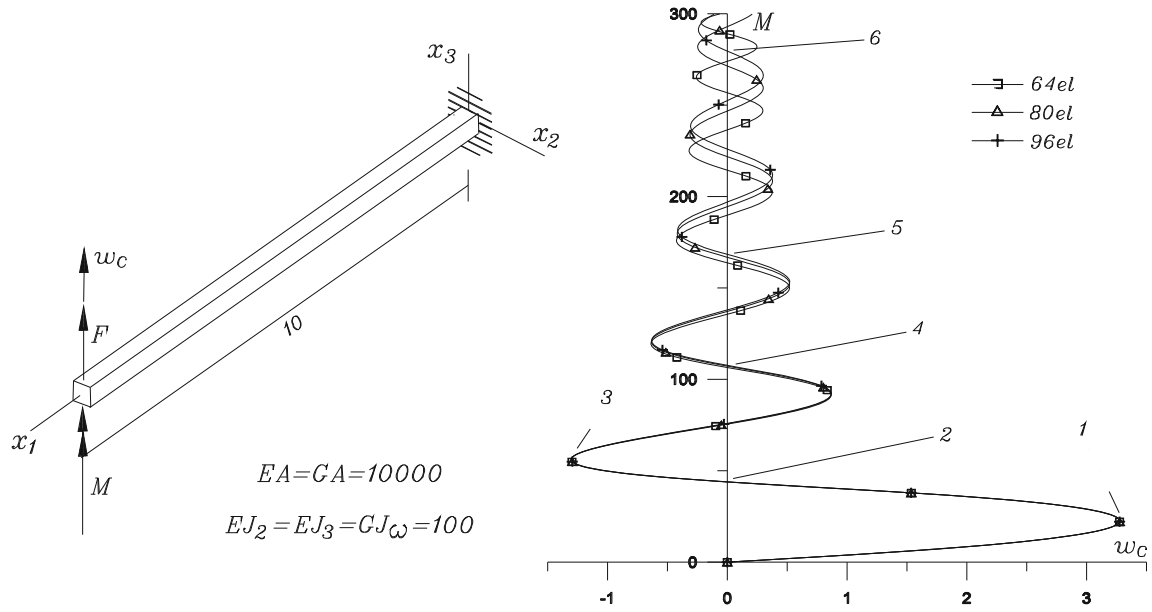

Fig. 9 Example 5: problem definition and equilibrium paths

$$d_\alpha[\mathbf{E}(\mathbf{r}+\alpha\delta\mathbf{r})]_{12} = d_\alpha(e_{21}+\alpha\delta e_{21}) = -\delta r_3 = -\delta\varphi_3 e_{22} + \delta\varphi_2 e_{23}. \tag{63}$$

Then, we obtain

$$\delta\mathbf{r} = \begin{bmatrix} e_{33} & 0 & -e_{31} \\ 0 & e_{33} & -e_{32} \\ 0 & -e_{23} & e_{22} \end{bmatrix} \delta\boldsymbol{\varphi} = \mathbf{A}(\mathbf{r})^{-1}\delta\boldsymbol{\varphi}. \tag{64}$$

The inverse relation of (64), by the $e_{11} = e_{22}e_{33} - e_{23}e_{32}$ evaluation used in the parametrization, leads to the searched expression

$$\delta\boldsymbol{\varphi} = \frac{1}{e_{11}e_{33}} \begin{bmatrix} e_{11} & e_{31}e_{23} & e_{31}e_{33} \\ 0 & e_{22}e_{33} & e_{32}e_{33} \\ 0 & e_{23}e_{33} & e_{33}^2 \end{bmatrix} \delta\mathbf{r} = \mathbf{A}(\mathbf{r})\delta\mathbf{r}. \tag{65}$$

From (64) and (65) it is clearly seen that $\mathbf{A}(\mathbf{r})^{-1}$ and $\mathbf{A}(\mathbf{r})$ operators are well defined in the assigned range of validity of the parametrization and that $\mathbf{A}(\mathbf{r})$ reduces to $\mathbf{I}$ as $\mathbf{r}$ goes to zero.

6 Applied moments, boundary conditions and solution scheme

In this section, after describing the treatment of the given external moments and boundary conditions, the system of the nonlinear equations and the adopted solution scheme are discussed.

As remarked in the previuos section, only the external work of forces can be defined in the described formulation so moments can be modelled as forces following the motion of points of the beam element. In particular, let vector $\overset{n}{\mathbf{m}}$ be the spatially fixed moment applied in the n node and $\overset{n}{\mathbf{g}}_i$ the related nodal basis. We also refer to the three points P_i on $\overset{n}{\mathbf{g}}_i$ at a fixed unit distance from the n node. Displacements of these points, therefore, are defined by referring to the (30) rigid motion as $\mathbf{u}_{(1)} = \bar{\mathbf{u}}(1,0,0)$, $\mathbf{u}_{(2)} = \bar{\mathbf{u}}(0,1,0)$ and $\mathbf{u}_{(3)} = \bar{\mathbf{u}}(0,0,1)$. Then, we have

$$\mathbf{u}_{(i)} = \overset{n}{\mathbf{u}} + \overset{n}{\mathbf{g}}_i - \hat{\mathbf{g}}_i, \tag{66}$$

where $\overset{n}{\mathbf{u}}$ is the displacement vector of the n node while the presence of the $\hat{\mathbf{g}}_i$ vectors will not have any influence.

We denote now by $\mathbf{p}_{(i)}$ three force vectors applied to the related P_i points. The force—$\sum_i \mathbf{p}_{(i)}$ is also applied to the n node to zeroing the resultant force vector. By (66), then, we compute the external work as

$$W_{\mathbf{m}} = \sum_i \mathbf{p}_{(i)}^T(\mathbf{u}_{(i)} - \overset{n}{\mathbf{u}}) = \sum_i \mathbf{p}_{(i)}^T(\overset{n}{\mathbf{g}}_i - \hat{\mathbf{g}}_i). \tag{67}$$

The variation of the functional $W_{\mathbf{m}}$ is carried out on the $\overset{n}{\mathbf{g}}_i$ vectors by considering $\mathbf{p}_{(i)}$ as constants. Then, after variation of (67) with respect to the rotational parameters chosen to represent the $\overset{n}{g}_{ij}$ components, we define the $\mathbf{p}_{(i)}$ force vectors by

$$\mathbf{p}_{(i)} = -\frac{1}{2}\sum_{jk} e_{ijk}\, p_j\, \overset{n}{\mathbf{g}}_k, \quad \sum_i \overset{n}{\mathbf{g}}_i \times \mathbf{p}_{(i)} = \overset{n}{\mathbf{m}}. \tag{68}$$

As can be observed in (68), applied forces are such that the resulting moment in the n node is the given $\overset{n}{\mathbf{m}}$ vector. Simple algebraic manipulations, finally, lead to the $p_i = \overset{n}{\mathbf{m}}^T \overset{n}{\mathbf{g}}_i$

Table 6 Example 5: computational characteristics for the A and S based parametrization algorithms

N_e	64			80			96		
$\bar{N}^{it}_{\lambda_{(1)}}$	$4_{1.0}$	$5_{1.5}$	$6_{1.5}$	$4_{1.0}$	$5_{1.5}$	$6_{1.5}$	$4_{1.0}$	$5_{1.5}$	$6_{1.5}$
A_1-parametrization, second order approximation									
	A_1-parametrization, second order approximation								
Steps	626	368		624	248		600	257	
N_m	4.021	4.893		4.019	4.927		4.020	4.934	
t	13.56	9.695		16.75	8.188		19.31	10.14	
	A_1-parametrization, fourth order approximation								
Steps	672	215	98	605	192	99	553	186	91
N_m	4.015	4.986	5.554	4.017	4.990	5.490	4.020	4.989	5.609
t	16.96	6.718	3.444	18.93	7.484	4.246	20.79	8.671	4.765
	Exact representation								
Steps	666	203	91	610	189	81	555	186	78
N_m	4.015	4.985	5.648	4.016	4.984	5.716	4.020	4.989	5.692
t	20.53	7.743	3.937	23.40	9.073	4.413	25.53	10.59	5.101
A_2-parametrization, second order approximation									
	A_2-parametrization, second order approximation								
Steps	750	278		623	315		602	311	
N_m	4.027	4.921		4.022	4.879		4.023	4.864	
t	16.03	7.250		16.56	10.13		19.17	11.96	
	A_2-parametrization, fourth order approximation								
Steps	680	217	168	582	198	95	546	191	80
N_m	4.015	4.982	4.966	4.019	4.985	5.694	4.020	4.990	5.925
t	16.46	6.609	5.046	17.64	7.500	4.155	19.76	8.625	4.313
	Exact representation								
Steps	655	204	75	591	196	82	577	190	77
N_m	4.015	4.971	5.760	4.019	4.969	5.524	4.017	4.974	5.675
t	18.60	7.140	3.063	21.23	8.578	4.001	23.84	9.969	4.625
S-parametrization, second order approximation									
	S-parametrization, second order approximation								
Steps	783	342		692	279		657	255	
N_m	4.011	5.088		4.013	5.018		4.014	4.957	
t	13.95	7.734		15.34	7.828		17.43	8.406	
	S-parametrization, fourth order approximation								
Steps	682	232	133	617	213	102	570	208	93
N_m	4.015	4.991	5.526	4.018	4.995	5.745	4.019	5.000	5.779
t	13.92	5.875	3.735	15.67	6.796	3.750	17.39	7.875	4.197
	Exact representation								
Steps	682	225	92	617	211	90	570	205	86
N_m	4.015	4.987	5.745	4.018	5.000	5.726	4.019	4.995	5.660
t	16.76	6.828	2.900	18.92	8.016	3.896	20.93	9.343	4.443

components. We note that, the definitions given in (67) and (68) imply that the external force vectors are a function of the assumed unknowns.

We emphasize that boundary conditions assigned to rotations are imposed directly because the three chosen parameters fully characterize the rigid configuration of the beam section for both slopes and angles based formulations. For the slopes based formulations, in particular, let $\overset{n}{\alpha}_i \mathbf{k}_i$ be the imposed rotation at the n node with an angle α_i about the $\mathbf{k}_i$ reference axis. By simple geometrical considerations the following relations between the fixed angle values and the the rotation parameters

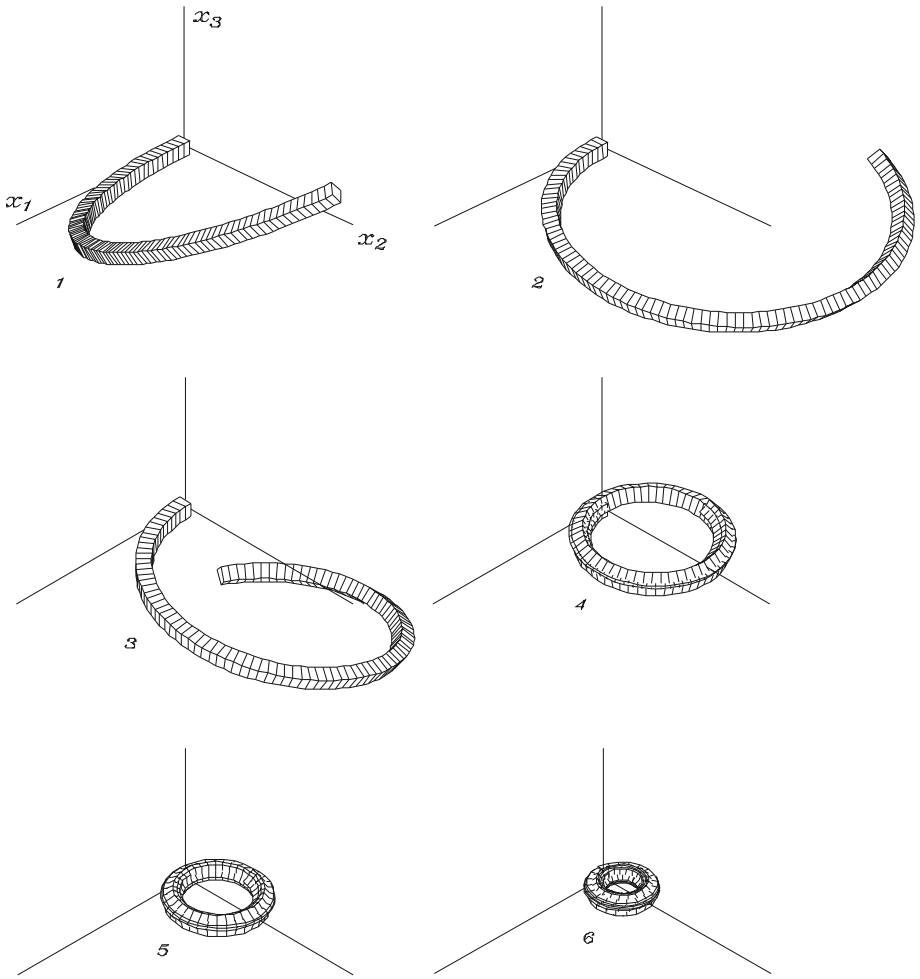

Fig. 10 Example 5: deformed configurations for N_e=96

$$\begin{aligned} \sin\overset{n}{\alpha}_1 &= \mathbf{k}_3 \times \overset{n}{\mathbf{g}}_3 \cdot \mathbf{k}_1 = -\overset{n}{g}_{32}, \\ \sin\overset{n}{\alpha}_2 &= \mathbf{k}_3 \times \overset{n}{\mathbf{g}}_3 \cdot \mathbf{k}_2 = \overset{n}{g}_{31}, \\ \sin\overset{n}{\alpha}_3 &= \mathbf{k}_2 \times \overset{n}{\mathbf{g}}_2 \cdot \mathbf{k}_3 = -\overset{n}{g}_{21}, \end{aligned} \tag{69}$$

are obtained. In effect, $\mathbf{k}_i \times \mathbf{g}_i$ is the value $\sin\alpha_i$ with α_i being the angle formed by $\mathbf{k}_i$ and $\mathbf{g}_i$. Subsequent projection on the choice $\mathbf{k}_i$ axis gives the imposed $\sin\alpha_i$ value. As an example, let a support allow the rotation about the directions $\mathbf{k}_2$ and $\mathbf{k}_3$ but not about $\mathbf{k}_1$. Such a condition, imposed at the n node, is described in terms of the chosen rotational parameters by $\overset{n}{g}_{32} = 0$. By the (69) expressions, finally, appears that no singularities occur in the boundary conditions imposition.

The definition of equilibrium equations is based on the stationary problem for the functional

$$\Pi(\mathbf{u}, \mathbf{r}) = U(\mathbf{u}, \mathbf{r}) - W(\mathbf{u}, \mathbf{r}), \tag{70}$$

with internal energy U and external work W. For each described two-node element, the three components u_i are the nodal displacements while r_i are the three nodal rotation parameters. In particular, for the slopes or the angles based descriptions respectively, components r_i represent the e_{21}, e_{31} and e_{32} slope or the ψ_1, ψ_2 and ψ_3 angle parameters. After discretization and inclusion of the boundary conditions, the $\delta\Pi$ variation of the functional leads to a system of nonlinear equations in the unknown vector $\mathbf{q}$. Therefore, by denoting with $\mathbf{N}(\mathbf{q})$ the internal force vector, the nonlinear equations are expressed by

$$\mathbf{N}(\mathbf{q}) - \lambda\mathbf{P} = 0. \tag{71}$$

In (71), $\mathbf{P}$ and λ are the external force vector and the external force parameter, respectively.

A predictor–corrector scheme as described in [23] for the equilibrium path individualization is used in the analysis. It is characterized by a predictor step obtained by the linear extrapolation of the previously computed $\mathbf{q}_{(k)}$ and $\mathbf{q}_{(k-1)}$ vectors when $k > 0$, while the first order asymptotic extrapolation is used when $k = 0$. Furthermore, the corrector is accomplished by a Newton method based corrector scheme with minimization of the distance between the approximate and equilibrium points as a constraint equation.

The length $\mu_{(k)}$ of the extrapolation parameter in the k-th predictor–corrector step is chosen as a function of the iterations $N^{it}_{(k-1)}$ performed in the previous corrector

step and a $\bar{N}^{it}$ target iteration count. Evaluation $\mu_{(k)} = \mu_{(k-1)}\bar{N}^{it}/N^{it}_{(k-1)}$ is adopted to save computational costs in the analysis because high $\mu_{(k)}$ values can be reached. However, restriction $\mu_{(k)}/\mu_{(k-1)} \leq 2$ is imposed in the code to avoid excessively long predictor steps.

The corrector process computes the increments of the l-th approximation of the force parameter $\Delta\lambda_{(l)}$ and vector of discretization parameters $\Delta\mathbf{q}_{(l)}$. It is stopped when the convergence criterion

$$\epsilon_{(l)} = \frac{\|\Delta\mathbf{q}_{(l)}\|}{\|\mathbf{q}_{(l)}\|} < 10^{-8} \tag{72}$$

is satisfied. If divergence in corrector iterations occurs, a new predictor–corrector step is performed with the length $\mu_{(k)}$ halved.

Detection of the bifurcation points along the equilibrium path traced by the used continuation method is obtained by the algorithm described in [24]. Basically, the algorithm begins the bifurcation points computation once their presence has been pointed out within a predictor–corrector step. The computation is initialized by solving a linear eigenvalues problem defined on the linear extrapolation. Then, the bifurcation points are exactly determined by solving the complete nonlinear system constituted by the equilibrium equation and the eigenvalue problem. Finally, the introduction of one further suitable equation makes the consequent augmented system well-posed.

7 Numerical examples

Some numerical tests have been carried out with the suggested algorithms. The described formulations based on slopes and angles for the parametrization of rotations, respectively S-parametrization and A-parametrization, have been compared. In particular, A_1-parametrization refers to the use of rotation matrix (13) while A_2-parametrization refers to the use of expression (18). predictor–corrector steps are characterized by the use of Newton's method as corrector with several $\bar{N}^{it}$ target iteration counts. Tables report the number (*steps*) of predictor–corrector steps, the (N_m) mean value of the number of Newton's iterations in the *steps* and the (t) CPU time (s) spent in the whole analysis.

In all tests the initial solution point is $(\mathbf{q}_{(0)}, \lambda_{(0)}) = (0, 0)$ while $\lambda_{(1)}$ initial λ-increments are assigned. Traversing a given displacement component or load parameter value is adopted as the stopping criteria of the continuation analysis. Divergence of the correction iteration is pointed out here by condition $\epsilon_{(l)} > \epsilon_{(l-1)}$ for $l > 1$. A maximum number of iterations ($N_{\max}$) are also permitted in the corrector step. In particular, $N_{\max}$=10 is assigned to indicate that the iteration process becomes very slow. Several refinement levels of the mesh obtained by using N_e elements are also tested.

When compared to reference results, similar equilibrium states computed by the described treatments of the finite rotations and beam element model are obtained. Additionally, the differences between the computed equilibrium paths computed by S and A like parametrizations are negligible. In effect, whereas the treatment of the rotations is different, the beam finite element used is the same. Finally, at present, we are primarily concerned with comparing the number of arithmetical operations and simplicity in programming rather than discretization error.

In the tests, due to the different range of validity of the approximation, $\bar{N}^{it}$=4,5 for the second order and $\bar{N}^{it}$=4,5,6 for the fourth order extrapolations and the exact representations of the rotation map is used. From the resulting behaviour of the Newton's iterations, however, we note that $\bar{N}^{it}$=6 is a limit value for the predictor steps evaluation. In effect, for such a value, $N_m \leq 5$ denotes that several divergences in the corrector steps or excessively long predictor steps occur before the analysis is completed.

7.1 Example 1: lateral buckling of a narrow cantilever beam

The narrow cantilever beam shown in Fig. 3 was analysed by meshes of 8, 12 and 16 elements. The numerical results obtained in Kouhia [20] and Battini and Pacoste [4] can be taken as reference. The $\lambda - w_c$ vertical load parameter − lateral tip displacement curves were computed and displayed as a ratio of $\gamma_o = \sqrt{EJ_3GJ_\omega}/L^2$ and L, $L = 100$, respectively. The analyses were stopped when the value $\lambda = 12$ was reached. Significant deformed configurations are also shown. Computational performances are reported in Table 1 in the cases of second order, fourth order and exact representations of the rotation map.

If the imperfection is removed, bifurcation points appear along the equlibrium path. The λ_b buckling loads are now calculated for increasing J_3/J_2 values of the aspect ratio of the cross section. The $\gamma_b = 4.0126\gamma_o/\lambda_b$ values are reported in Table 2 and refer to meshes of 8, 16 and 32 elements in the cases of exact S-representations of the rotation map. Furthermore, to take into account high values of the aspect ratio, the torsion constant is calculated from the five term approximation

$$J_\omega = \frac{1}{3}h_2h_3^3\left\{1 - \frac{192}{\pi^5}\frac{h_3}{h_2}\sum_{n=1}^{4}\frac{1}{(2n-1)^5}\tanh\left[\frac{\pi}{2}\frac{h_2}{h_3}(2n-1)\right]\right\}. \tag{73}$$

To compute accurate buckling load values over a large range of the aspect ratio, a numerical integration on the exact buckling load formula was carried out in Hodges and Peters

[16], while finite element approaches with an additive and a multiplicative representation in the update procedure was used in [9] and Lee et al. [22], respectively. In particular, to avoid complexity in the formulation, in [9] the second derivative of the $\mathbf{A}(\boldsymbol{\psi})$ operator is neglected in the stiffness matrix definition.

The γ_b values here computed by using the 32 elements mesh are compared with the cited results in Fig. 4. When the pre-buckling deflections are negligible there are no significant differences in the buckling loads depending on which approach is used. The prebuckling deformations will become large as the value J_3/J_2 increases. In these cases, the approximation $\mathbf{A}(\boldsymbol{\psi}) = \mathbf{I}$ operated for the second derivative in the tangent matrix calculation is not longer valid and the related detection of the critical points is not accurate.

7.2 Example 2: right-angled frame under an end load

The nonlinear solution path of the L frame shown in Fig. 5 is analysed. This example, first proposed by Argyris et al. in [2], has been analysed with nonlinear shell elements in Wriggers and Gruttmann [39]. The finite dimension connection between the members of the frame was modelled in [4] with both a rigid and disregard connections. The $\lambda - w_c$ horizontal load parameter − lateral tip displacement of the free end curves was computed until the $\lambda = 4$ value and displayed. Significant deformed configurations are also shown in Fig. 5. The analysis refers to a total number of 8, 16 and 24 elements used in the frame. Computational characteristics are reported in Table 3.

7.3 Example 3: right-angled frame under end moments

In this example the right angle frame depicted in Fig. 6 is analysed. Appreciable large rotations with a significant amount of twist are considered. The loading is given by a pair of concentrated moments applied at the supports. Due to the symmetry, only half of the frame is modelled. At the support only translation along x_1 and rotation around x_3 are allowed. The $\lambda - w_c$ moment parameter − apex displacement in the x_3 direction diagram and several deformed configurations are plotted. The results are in agreement with those found in [4] and [40]. Equilibrium points and computational performances, reported respectively in Fig. 6 and in Table 4, refer to meshes with 6, 12 and 18 elements for the half of the frame.

By using S parametrization and N_e=18, the test is also carried out by removing the imperfection load after the first buckling phase as in [34]. In the analysis, therefore, the equilibrium curve traverses the negative critical point and completes a second revolution of the frame about the line connecting its hinged ends. Applied moment versus lateral displacement curves are shown in Fig. 7 for the first and second revolution. Afterward computed solution points traverse the positive critical point and describe the same first post-buckling behaviour as previously computed. In the S formulation, then, there is no difficulty in subjecting the frame to any number of revolutions. A symmetrical intersection of the moment axis is, furthermore, obtained. Again in Fig. 7, the curves $\lambda - g_{ij}$ components of the director $\mathbf{g}_1^b$ at the hinged point and $\mathbf{g}_2^c$ and $\mathbf{g}_3^c$ at the apex are shown.

Table 7 Example 5, $F = 0$ case: free-end displacements under end moment obtained by exact S-representation and analytic solution

M	N_e=16	N_e=32	N_e=64	analytic
u_{c1} Displacement component				
7.85398	−0.996709	−0.996805	−0.996829	−0.996837
15.7080	−3.64152	−3.63572	−3.63428	−3.63380
23.5619	−7.03299	−7.00739	−7.00105	−6.99895
31.4159	−10.0651	−10.0161	−10.0040	−10
39.2699	−11.8578	−11.8150	−11.8042	−11.8006
47.1239	−12.0931	−12.1160	−12.1206	−12.1221
54.9779	−11.1136	−11.2458	−11.2762	−11.2862
62.8319	−9.73029	−9.93494	−9.98389	−10
70.6858	−8.81297	−8.94916	−8.97697	−8.99965
78.5398	−8.84544	−8.74068	−8.72941	−8.72676
86.3938	−9.67332	−9.28178	−9.20529	−9.18153
94.2478	−10.6132	−10.1484	−10.0364	−10
u_{c2} Displacement component				
7.85398	3.73096	3.72966	3.72934	3.72923
15.7080	6.37462	6.36830	6.36672	6.36620
23.5619	7.25105	7.24666	7.24556	7.24519
31.4159	6.33447	6.35846	6.36428	6.36620
39.2699	4.23987	4.32097	4.34062	4.34711
47.1239	1.94968	2.07987	2.11157	2.12207
54.9779	0.388318	0.496124	0.523567	0.532747
62.8319	0.0235037	0.0013368	0.0000817	0
70.6858	0.678260	0.471916	0.428262	0.414359
78.5398	1.66023	1.36578	1.29605	1.27324
86.3938	2.17235	2.04060	1.99275	1.97596
94.2478	1.80994	2.08786	2.11565	2.12207

7.4 Example 4: deep circular arch under vertical load

This test concerns the deep arch problem shown in Fig. 8. This example was analysed in [34] and Kouhia and Mikkola [21] for the two-dimensional and in Cardona and Huespe [10] for the 3D behaviour. Meshes with 24, 36 and 48 equal elements for the whole arch are employed. The frame is subjected to point loads, respectively λ along the x_2 and $\epsilon\lambda$ along the x_3 direction, in the apex. The arch is fully clamped at one end and only the in plane x_1x_2 rotation is permitted at the other end.

The analysis is stopped when the vertical deflection of the apex value $v_c = 200$ is traversing. The λ - v_c equilibrium path and some deformed configurations are shown in Fig. 8. As usual, computational performances are reported in Table 5 for Newton corrector and several imposed $\bar{N}^{it}$ iterations.

7.5 Example 5: beam bent to a helical form

The cantilever beam shown in Fig. 9 was analysed by meshes of 32, 64 and 96 elements. This example, introduced by Ibrahimbegović [17] and also analysed in [4], illustrates the effects of the simultaneous application of a bending moment and a transversal load. In particular, the beam is subjected to a concentrated moment $\mathbf{M} = 120\pi\lambda\mathbf{k}_3$ and an out-of-plane force $\mathbf{F} = 30\lambda\mathbf{k}_3$ applied at its free end.

In the cited works the out-of-plane x_3-displacement oscillates around a zero value, while each passing through zero corresponds to a deformed shape which is entirely situated in the plane x_1x_2. Not all rotation parametrizations are able to trace the true equlibrium path. As noted in [4], attention must be paid to the external moment definition because different parameterisations of rotations will imply different physical definitions of $\mathbf{M}$. As a consequence, the results obtained using different types of parameterisation will be completely different.

Here we adopt the applied moments definition given in Sec. 5 for both S and A like parametrizations while $\mathbf{g}_i$ vectors are computed by the related rotation maps. It follows that, also in this test, almost identical equilibrium states computed by the described treatments of the finite rotations are obtained.

The M - w_c moment value - out-of-plane tip displacement curves were computed and also shown in Fig. 9. The analyses were stopped when the value $M = 300$ was reached. Significant deformed configurations in the specified points of Fig. 9 are shown in Fig. 10. Computational performances are reported in Table 6 for second order, fourth order and exact representations of the rotation maps.

In the $F = 0$ case, the only non-trivial deformation component is the flexural one. According to the classical Euler formula, this bending deformation is constant along the beam. The analytic solution for the free-end rotation and displacement components can be obtained respectively as

$$\alpha_{c3} = \frac{ML}{EJ_3} \tag{74}$$

and

$$u_{c1} = L - \frac{L}{\alpha_{c3}/2}\sin\frac{\alpha_{c3}}{2}\cos\frac{\alpha_{c3}}{2}, \quad u_{c2} = \frac{L}{\alpha_{c3}/2}(\sin\frac{\alpha_{c3}}{2})^2, \tag{75}$$

where $L = 10$. In Table 7 the free-end displacements obtained by the analytic solution and the numerical exact S-representation are compared. In particular, numerical results are obtained by using $\Delta\lambda_{(k)} = 0$ as constraint equation and $\mu_{(k)} = 1$ as extrapolation length for any k-th predictor–corrector step. Initial solution point is computed for the $M = 2.5\pi/10$ bending moment value while results refer to each ten steps. The solution for the rotation and $u_{c3} = 0$ values are not reported because identical to the analytic one for each of the used meshes. Then, by Table 7, we can see that the presented formulation is capable of representing the classical solution of Euler.

8 Conclusions

In the hypothesis of large displacements and rotations and small strains, a technique to analyse the behaviour of 3D finite element beam frames has been presented. By utilizing vectorial operations, the approach is based on an updated Lagrangian description of rotations. The described formulation does not use angle measures and we have validated that it is capable to follow any finite rotations.

The treatment of rotational boundary conditions and external moments proves to be slightly more complex with respect to the co-rotational formulations. Furthermore, the incremental rotations are restricted to the range of validity of the described parametrization. However, computationally, efficient expressions in the equations of the nonlinear system are obtained. Furthermore, case statements are not present in the coding of the presented formulation. In the numerical tests a similar number of predictor–corrector steps to complete the analysis for both S and A like parametrizations was used. Hence, fewer arithmetical operations and less implementation effort with respect to the classical one is required.

Overall, the proposed formulation shows simplicity of the analysis while computational effectiveness and algorithmic reliability are retained.

9 Appendix 1: Regularity of the augmented constrained problem

The nine $g_{i,j}$ unknown components of the $\mathbf{g}_i$ vectors are subject to six constraint conditions. We demonstrate here that the rotational degrees of freedom are reduced just to three. Of course, six conditions being imposed, the degrees of freedom are at least three. To show also that the degrees of freedom are at most three we refer to the definitions $i_- = i - 1$ and $i_+ = i + 1$ for the cyclic sequence of the Latin indices.

The constraint equations are

$$\mathbf{g}_2 \cdot \mathbf{g}_2 - 1 = 0,$$
$$\mathbf{g}_3 \cdot \mathbf{g}_3 - 1 = 0,$$
$$\mathbf{g}_2 \cdot \mathbf{g}_3 = 0,$$

$$\mathbf{g}_2 \times \mathbf{g}_3 = \mathbf{g}_1, \tag{76}$$

where the related Jacobian matrix is denoted by $\mathbf{H}$. We show that nullity($\mathbf{H}$) is at most three in the solution point. The open mapping theorem then gives the result. The Jacobian matrix of the system (76) is

$$\mathbf{H} = \begin{bmatrix} 0\,0\,0 & g_{2,1} & g_{2,2} & g_{2,3} & 0 & 0 & 0 \\ 0\,0\,0 & 0 & 0 & 0 & g_{3,1} & g_{3,2} & g_{3,3} \\ 0\,0\,0 & g_{3,1} & g_{3,2} & g_{3,3} & g_{2,1} & g_{2,2} & g_{2,3} \\ 1\,0\,0 & 0 & -g_{3,3} & g_{3,2} & 0 & g_{2,3} & -g_{2,2} \\ 0\,1\,0 & g_{3,3} & 0 & -g_{3,1} & -g_{2,3} & 0 & g_{2,1} \\ 0\,0\,1 & -g_{3,2} & g_{3,1} & 0 & g_{2,2} & -g_{2,1} & 0 \end{bmatrix} \tag{77}$$

Then, in the solution point and for a given known vector $\mathbf{z}$, we must verify that six of the nine $y_{i,j}$ components of the unknown vector $\mathbf{y}$ are uniquely determinable from the system $\mathbf{H}\mathbf{y} = \mathbf{z}$.

From the last three rows of the system, as we can see in (77), the $y_{1,i}$ unknowns are easy to calculate. Therefore the system is reduced to the form

$$\begin{bmatrix} g_{2,1} & g_{2,2} & g_{2,3} & 0 & 0 & 0 \\ 0 & 0 & 0 & g_{3,1} & g_{3,2} & g_{3,3} \\ g_{3,1} & g_{3,2} & g_{3,3} & g_{2,1} & g_{2,2} & g_{2,3} \end{bmatrix} \begin{Bmatrix} y_{2,1} \\ y_{2,2} \\ y_{2,3} \\ y_{3,1} \\ y_{3,2} \\ y_{3,3} \end{Bmatrix} = \begin{Bmatrix} z_2 \\ z_3 \\ z_{2,3} \end{Bmatrix}. \tag{78}$$

For at least one i and one j is $g_{2,i} \neq 0$ and $g_{3,j} \neq 0$, respectively. Then, from the first two rows of (78) we obtain

$$\begin{aligned} y_{2,i} &= (z_2 - g_{2,i-}y_{2,i-} - g_{2,i+}y_{2,i+})/g_{2,i}, \\ y_{3,i} &= (z_3 - g_{3,j-}y_{3,j-} - g_{3,j+}y_{3,j+})/g_{3,j}. \end{aligned} \tag{79}$$

By inserting (79) in the third row of system (78) and multiplying by $g_{2,i}g_{3,j}$ it follows that

$$\begin{aligned} &[g_{2,i}g_{3,i-} - g_{2,i-}g_{3,i}]g_{3,j}y_{2,i-} \\ &\quad +[g_{2,i}g_{3,i+} - g_{2,i+}g_{3,i}]g_{3,j}y_{2,i+} \\ &\quad +[g_{2,j-}g_{3,j} - g_{2,j}g_{3,j-}]g_{2,i}y_{3,j-} \\ &\quad +[g_{2,j+}g_{3,j} - g_{2,j}g_{3,j+}]g_{2,i}y_{3,j+} \\ &= c_1 g_{3,j}y_{2,i-} + c_2 g_{3,j}y_{2,i+} \\ &\quad +c_3 g_{2,i}y_{3,j-} + c_4 g_{2,i}y_{3,j+} = \bar{z}, \end{aligned} \tag{80}$$

with coefficients $c_1, \ldots, c_4$ and $\bar{z}$.

At the solution, the last three equations in (76) give

$$g_{2,k}g_{3,k+} - g_{2,k+}g_{3,k} = g_{1,k-}. \tag{81}$$

In particular, (81) with

$$\begin{aligned} &k = i- \quad \Rightarrow g_{2,i-}g_{3,i} - g_{2,i}g_{3,i-} = g_{1,i+} \\ &\quad \Rightarrow c_1 = -g_{1,i+}; \\ &k = i \quad \Rightarrow g_{2,i}g_{3,i+} - g_{2,i+}g_{3,i} = g_{1,i-} \\ &\quad \Rightarrow c_2 = g_{1,i-}; \\ &k = j- \quad \Rightarrow g_{2,j-}g_{3,j} - g_{2,j}g_{3,j-} = g_{1,j+} \\ &\quad \Rightarrow c_3 = g_{1,j+}; \\ &k = j \quad \Rightarrow g_{2,j}g_{3,j+} - g_{2,j+}g_{3,j} = g_{1,j-} \\ &\quad \Rightarrow c_4 = -g_{1,j-}; \end{aligned}$$

so (80) becomes

$$\begin{aligned} &-g_{1,i+}g_{3,j}y_{2,i-} + g_{1,i-}g_{3,j}y_{2,i+} + g_{1,j+}g_{2,i}y_{3,j-} \\ &\quad -g_{1,j-}g_{2,i}y_{3,j+} = \bar{z}. \end{aligned} \tag{82}$$

In the case of $i \neq j$, as all components of $\mathbf{g_1}$ are present at least one coefficient in (82) is not zero and an unknown is definite.

The case $i = j$ implies that if $g_{1,i-} \neq 0$ or $g_{1,i+} \neq 0$, as before, an unknown is definite. Otherwise, if $g_{1,i-} = g_{1,i+} = 0$ we have that $g_{1,i} \neq 0$. Then, from (81) with $k = i+$ we have

$$g_{2,i+}g_{3,i-} - g_{2,i-}g_{3,i+} = g_{1,i} \neq 0, \tag{83}$$

while with $k = i$ and $k = i-$ is

$$g_{2,i}g_{3,i+} - g_{2,i+}g_{3,i} = g_{1,i-} = 0 \tag{84}$$

and

$$g_{2,i-}g_{3,i} - g_{2,i}g_{3,i-} = g_{1,i+} = 0, \tag{85}$$

respectively. But, by computing $g_{3,i+}$ and $g_{3,i-}$ from (84) and (85) respectively, and inserting this in (83) we have

$$g_{2,i+}\frac{g_{2,i-}g_{3,i}}{g_{2,i}} - g_{2,i-}\frac{g_{2,i+}g_{3,i}}{g_{2,i}} \neq 0, \tag{86}$$

that is, the false condition

$$g_{3,i}(g_{2,i+}g_{2,i-} - g_{2,i-}g_{2,i+}) \neq 0. \tag{87}$$

References

1. Argyris J (1982) An excursion into large rotations. Comput Methods Appl Mech Eng 32:85–155
2. Argyris J et al (1979) Finite element method: the natural approach. Comput Methods Appl Mech Eng 17(18):1–106
3. Atluri SN, Cazzani A (1995) Rotations in computational solid mechanics. Arc Comput Methods Eng 2:49–138
4. Battini JM, Pacoste C (2002) Co-rotational beam elements with warping effects in instability problems. Comput Methods Appl Mech Eng 191:1755–1789
5. Belytschko T, Hsieh BJ (1973) Non-linear transient finite element analysis with convected co-ordinates. Int J Numer Methods Eng 7:255–271
6. Betsch P, Steinmann P (2001) Constrained integration of rigid body dynamics. Comput Methods Appl Mech Eng 191:467–488
7. Betsch P, Steinmann P (2003) Constrained dynamics of geometrically exact beams. Comput Mech 31:49–59
8. Campello EMB, Pimenta PM, Wriggers P (2011) An exact conserving algorithm for nonlinear dynamics with rotational DOFs and general hyperelasticity. Part 1: shells. Comput Mech 48:195–211
9. Cardona A, Geradin M (1988) A beam finite element non-linear theory with finite rotations. Int J Numer Methods Eng 26:2403–2438

10. Cardona A, Huespe A (1999) Evaluation of simple bifurcation points and post-critical path in large finte rotation problems. Comput Methods Appl Mech Eng 175:137–156
11. Crisfield MA (1990) A consistent co-rotational formulation for nonlinear three-dimensional beam elements. Comput Methods Appl Mech Eng 81:131–150
12. Dufva KE, Sopanen JT, Mikkola AK (2006) Three-dimensional beam element based on a cross-sectional coordinate system approach. Nonlinear Dyn 43:311–327
13. Felippa CA (2000) A systematic approach to the element-independent corotational dynamics of finite elements. Technical report CU-CAS-95-06. University of Colorado, Boulder
14. Geradin M, Rixen D (1995) Parametrization of finite rotations in computational dynamics: a review. Revue Eur des Elements Finis 4:497–553
15. Goldstein H (1980) Classical mechanics. Addison-Wesley, Reading
16. Hodges DH, Peters DA (1975) On the lateral buckling of uniform slender cantilever beams. Int J Solids Struct 11:1269–1280
17. Ibrahimbegović A (1997) On the choice of finite rotation parameters. Comput Methods Appl Mech Eng 149:49–71
18. Ibrahimbegović A, Al Mikdad M (1998) Finite rotations in dynamics of beams and implicit time-stepping schemes. Int J Numer Methods Eng 41:781–814
19. Ibrahimbegović A, Shakourzadeh H, Batoz JL, Guo YQ (1996) On the role of geometrically exact and second-order theories in buckling and post-buckling analysis of three-dimensional beam structures. Comput Struct 61:1101–1114
20. Kouhia R (1991) On kinematical relations of spatial framed structures. Comput Struct 40:1185–1191
21. Kouhia R, Mikkola M (1989) Tracing the equilibrium path beyond simple critical points. Int J Numer Methods Eng 28:2923–2941
22. Lee H, Jung DW, Jeong JH, Im S (1994) Finite element analysis of lateral buckling for beam structures. Comput Struct 53:1357–1371
23. Lopez S (2000) An effective parametrization for asymptotic extrapolations. Comput Methods Appl Mech Eng 189:297–311
24. Lopez S (2002) Detection of bifurcation points along a curve traced by a continuation method. Int J Numer Methods Eng 53:983–1004
25. Lopez S (2010) Structural dynamical analysis by a lengths-based description of the small strains in the finite displacements regime. Nonlinear Dyn 59:29–44
26. Lopez S (2010) A three-dimensional beam element undergoing finite rotations based on slopes and distance measures. Internal report 53. Dipartimento di Modellistica per l'Ingegneria, Università della Calabria, Rende
27. Lopez S (2012) Relaxed representations and improving stability in time-stepping analysis of three-dimensional structural nonlinear dynamics. Nonlinear Dyn 69:705–720
28. Lopez S, La Sala G (2010) A finite element approach to statical and dynamical analysis of geometrically nonlinear structures. Finite Elem Anal Des 46:1093–1105
29. Mohri F, Azrar L, Potier-Ferry M (2001) Flexuraltorsional post-buckling analysis of thin-walled elements with open sections. Thin Walled Struct 39:907–938
30. Mohri F, Damil N (2008) Large torsion finite element model for thin-walled beams. Comput Struct 86:671–683
31. Pimenta PM, Campello EMB, Wriggers P (2008) An exact conserving algorithm for nonlinear dynamics with rotational DOFs and general hyperelasticity. Part 1: rods. Comput Mech 42: 715–732
32. Rankin CC, Nour-Omid B (1988) The use of projectors to improve finite element performance. Comput Struct 30:257–267
33. Rhim J, Lee W (1998) A vectorial approach to computational modelling of beams undergoing finite rotations. Int J Numer Methods Eng 41:527–540
34. Simo JC, Vu-Quoc L (1986) A three-dimensional finite-strain rod model. Part II: computational aspects. Comput Methods Appl Mech Eng 58:79–116
35. Sopanen JT, Mikkola AM (2003) Description of elastic forces in absolute nodal coordinate formulation. Nonlinear Dyn 34:53–74
36. Spurrier RA (1978) Comments on singularity-free extraction of a quaternion from a director-cosine matrix. J Spacecr 15:255–256
37. Stuelpnagel J (1964) On the parameterization of the three-dimensional rotation group. SIAM Rev 6:422–430
38. Sugiyama H, Gerstmayr J, Shabana AA (2006) Deformation modes in the finite element absolute nodal coordinate formulation. J Sound Vib 298:1129–1149
39. Wriggers P, Gruttmann F (1993) Thin shells with finite rotations formulated in Biot stresses: theory and finite element formulation. Int J Numer Methods Eng 36:2049–2071
40. Yang YB, Lin SP, Chen CS (2007) Rigid body concept for geometric nonlinear analysis of 3D frames, plates and shells based on the updated Lagrangian formulation. Comput Methods Appl Mech Eng 196:1178–1192